A.R.A.P. REPORT 199 NASA CR-132323

SOME ANALYSES OF THE CHEMISTRY AND DIFFUSION OF SST EXHAUST MATERIALS DURING PHASE III OF THE WAKE PERIOD

Glenn R. Hilst
Coleman duP. Donaldson
Ross Contiliano

Prepared under Contract NAS1-11873 by
Aeronautical Research Associates of Princeton, Inc.
50 Washington Road, Princeton, New Jersey 08540

for

NATIONAL AERONAUTICS AND SPACE ADMINISTRATION

July 1973

A.R.A.P. REPORT 199 NASA CR-132323

SOME ANALYSES OF THE CHEMISTRY AND DIFFUSION OF SST EXHAUST MATERIALS DURING PHASE III OF THE WAKE PERIOD

Glenn R. Hilst
Coleman duP. Donaldson
Ross Contiliano

Prepared under Contract NAS1-11873 by
Aeronautical Research Associates of Princeton, Inc.
50 Washington Road, Princeton, New Jersey 08540

for

NATIONAL AERONAUTICS AND SPACE ADMINISTRATION

July 1973

ABSTRACT

In the generally stably stratified lower stratosphere, SST exhaust plumes could spend a significant length of time in a relatively undispersed state. During this time, the SST exhaust materials behave quite differently than had been proposed in earlier studies of their potential environmental impact. It is evident that these prior evaluations have uniformly adopted a conservative set of assumptions, in the sense that they maximize the effect of SST operations on the stratospheric environment. This report describes the first year of activity in an effort to develop more exact methods for CIAP evaluations.

This effort has utilized invariant modeling techniques to simulate the separate and combined effects of atmospheric turbulence, turbulent diffusion, and chemical reactions of SST exhaust materials in the lower stratosphere. The primary results to date are:

1. The combination of relatively slow diffusive mixing and rapid chemical reactions during the Phase III wake period minimizes the effect of SST exhausts on O_3 depletion by the so-called NO_x catalytic cycle. While the SST-produced NO is substantially above background concentrations, it appears diffusive mixing of NO and O_3 is simply too slow to produce the O_3 depletions originally proposed.

2. The time required to dilute the SST exhaust plume may be a significant fraction of the total time these materials are resident in the lower stratosphere. If this is the case, then prior estimates of the environmental impact of these materials must be revised significantly downward.

SOME ANALYSES OF THE CHEMISTRY AND DIFFUSION OF SST EXHAUST MATERIALS DURING PHASE III OF THE WAKE PERIOD

Glenn R. Hilst
Coleman duP. Donaldson
Ross Contiliano

Aeronautical Research Associates of Princeton, Inc.

SUMMARY

In the summer of 1972 the Aeronautical Research Associates of Princeton, Inc., (A.R.A.P.) undertook a study of the combined problems of atmospheric diffusion and chemical reactions associated with the potential impact of SST exhaust materials on the environmental properties of the lower stratosphere. This work was supported under Contract NAS1-11873, by a transfer of funds from the Department of Transportation's Climatic Impact Assessment Program (DOT/CIAP) to the National Aeronautics and Space Administration's Langley Research Center (NASA/LRC), and was directed by Dr. Alan Grobecker and Dr. Robert Underwood for DOT/CIAP and Dr. Robert Levine for NASA/LRC. The present document is a report on the first year of activity in this program and is directed to the technical results derived from applications of invariant model simulations of the separate and combined effects of atmospheric turbulence, turbulent diffusion, and chemical reactions to the problems of the behavior of SST exhaust materials during the time they are being diffused to background concentrations. In addition to these analyses, A.R.A.P. has participated actively in the CIAP programs of monograph preparations, workshops, and formal conferences.

The genesis and impetus for A.R.A.P.'s contributions to the DOT/CIAP analyses may be traced to the combination of Donaldson's development of second-order closure techniques for simulation of nonlinear dynamical systems (ref. 5), the prior application of these techniques to chemical kinetic processes in turbulent fluids by Donaldson and Hilst (ref. 4), and the recognition of the probability that, in the generally stably stratified lower stratosphere, SST exhaust plumes could spend a significant length of time in a relatively undispersed state. The combination of these events led to the conclusion that there was a very real possibility that during a significant part of their residence time in the lower stratosphere SST exhaust materials would behave quite differently

than had been proposed in the earlier studies of their potential environmental impact. In a very real sense, the studies reported here have attempted to test the bases of these earlier analyses and, where these have been found to be inadequate or erroneous, to develop more exact methods for the CIAP evaluations.

The results of these studies to date may be summarized as follows:

1. A detailed examination of the chemical depletion of ozone (O_3) by the so-called NO_x catalytic cycle during the time the SST exhausts are confined to above-background concentrations (the Phase III wake period in CIAP parlance) shows the combination of relatively slow diffusive mixing and rapid chemical reactions serves to minimize the effect of SST exhausts on O_3 depletion. While the SST produced NO is substantially above background concentrations, it appears diffusive mixing of NO and O_3 is simply too slow to produce the O_3 depletions originally proposed. By way of analogy, it is as though the SST exhaust NO were placed in the stratosphere in a slightly permeable "bag" which expands and erodes with time.

2. The time required to dilute the SST exhaust plume (the expansion and erosion of the analogous "bag" containing these materials) may be a significant fraction of the total time these materials are resident in the lower stratosphere. If this is the case, then prior estimates of the environmental impacts of these materials must be revised significantly downward.

The combination of these conclusions must be tempered by a clear recognition of the uncertainties of present knowledge and demonstrable facts which plague any analysis of this kind. These are detailed in the present report. However, it is evident that prior evaluations have uniformly adopted a conservative set of assumptions, in the sense that they lead to estimations of the maximum effect SST operations could have on the stratospheric environment. In the face of ignorance and uncertainty, this is, perhaps, a "safe" course to follow. A much more rational course, however, is to remove the ignorance and minimize the uncertainties, so that we might evaluate these effects confidently.

INTRODUCTION

In prior evaluations of the potential environmental impact of fleet operations of the SST in the lower stratosphere (refs. 1, 2, 3), it was assumed that the exhaust products from many flights were, somehow, conserved and uniformly mixed globally in a layer of the stratosphere. It was further assumed that natural constituents of this atmospheric layer, such as O_3, were also uniformly mixed with the exhaust products according to their local mean value. Under

these assumptions it was possible to calculate alterations of the equilibrium concentrations of natural constituents, and assess the changes in these values which should associate with routine SST fleet operations of N aircraft emitting a known amount of each exhaust material.

As a first approximation to the true state of affairs, these analysis techniques provided the first identification of the major potential impact of SST exhausts on the O_3 balance in the lower stratosphere and their possible effects on the radiation balance for incoming ultra violet light and on the circulations of the atmosphere which control weather and climate. These initial estimates suggested that either or both of these effects could be significant, and a more detailed analysis, which would refine these estimates, was in order before unlimited SST operations were undertaken.

In undertaking this more detailed analysis, the DOT/CIAP effort has, among other things, reopened the question of the validity of the assumptions of uniformly mixed SST exhaust and environmental constituents, and the work reported here is specifically directed to this facet of the CIAP evaluation. The need for a reexamination of these assumptions is readily established from a qualitative recognition of the distribution of exhaust products emitted continuously from multiple flights over a long period of time. Far from being uniformly distributed over the globe, the concentrations of these materials will vary from very high concentrations in the most recent exhaust plume to background concentrations where these exhaust materials rarely go. The range of concentrations between these two extremes can readily exceed four or five orders of magnitude. Intermediate between the extremes are the exhaust materials emitted during the prior days, weeks, and months, each in its appropriate stage of dilution to the background or uniformly mixed level of concentration.

At any one time, then, the more appropriate picture of the distribution of exhaust products in the lower stratosphere is one of considerable spatial inhomogeneity, superimposed upon any natural variability of the exhaust material under study. Now consider that the rate of reaction between two chemical species is, in the simplest case, proportional to their joint local concentrations. Then the total reaction rate in some volume of the atmosphere (say a spherical shell located in the lower stratosphere) is the volume integral of the product of the local concentrations of the reacting chemical species. If one of these species is uniformly distributed through this volume, the inhomogeneous distribution of the other does not alter the total reaction rate. However, if both species are inhomogeneously distributed, then the total reaction rate depends upon how they are mixed together, and may be very different from the rate predicted by assuming uniform values of concentration for either or both of the reacting species.

It is the purpose of the present study to quantify the above qualitative arguments and present an initial evaluation of the effect that inhomogeneous distributions of exhaust products have on the depletion of O_3 by the NO_x catalytic cycle during the time individual SST plumes are in the so-called Phase III wake phase. (This phase is defined as the time from vortex decay behind the aircraft until the SST plume has either grown to lateral dimensions of the order of 1000 km or the plume material is diluted by diffusive mixing to background concentrations and is, therefore, no longer distinguishable as an entity.)

The NO_x-O_3 reaction system has been selected because of its prime importance to the CIAP evaluation. Also, in order to provide maximum utility to the CIAP effort, the analyses are cast in terms of the chemical efficiency of NO destruction of O_3 during the Phase III wake phase, and the duration of this phase of the SST plume life. When analyzed in terms of the expected residence time for SST exhausts in the lower stratosphere, these measures of the chemical efficiency and duration of the wake phase permit an assessment of the effects of inhomogeneous concentration distributions on the overall estimate of O_3 depletion in the stratosphere.

Finally, the reader should be aware that novel and rather sophisticated modeling techniques have been employed in these analyses. In particular, coupled, second-order closure chemistry and diffusion models are used throughout. The models and their limitations are described in this report, but the reader interested in their development is referred to refs. 4, 5, and 6 for that information.

The Questions Posed

For the purposes of the DOT/CIAP evaluation we wish to address three related but specific questions:

1. During the Phase III wake period, is the chemical behavior of the SST exhaust materials significantly different from their behavior after they are well-mixed in the stratospheric environment?

2. If the answer to 1. is "yes," what is the nature and magnitude of this effect(s), and how long does it last?

3. Do the combinations of the nature, magnitude, and duration of the chemical behavior of SST exhausts during Phase III significantly alter estimates of the impact of SST fleet operations on the stratospheric environment?

Our primary objective here is to provide, within the limits of present knowledge, time, and resources, best estimates of the answers to questions 1. and 2. and, by comparison with large-scale global modeling, draw inferences regarding the answers to the third question. A secondary objective is to provide estimates of the diffusive growth and chemical behavior of SST exhaust plumes until they have reached the dimensions of the global transport and chemistry models. In this sense, these Phase III analyses serve as sub-grid scale models for the global models.

In order to make these results as specific as possible, we have focussed on the apparently critical problem of the destruction of O_3 by the NO_x catalytic cycle as described by Johnston (ref. 3). The analytical models used do not admit simultaneous solutions for a large number of reactions (because of excessive computational requirements). Our simulation of the NO_x catalytic cycle is therefore a simplified one which treats only the simultaneous diffusive mixing and reaction of O_3 with NO under the assumption of the immediate restoration (and therefore conservation) of NO by the reaction of NO_2 with O. Such an analytical system cannot, of course, pretend to follow all of the factors which contribute to the quasi-equilibrium concentrations of O_3 in the lower stratosphere. However, as shown later, the combined diffusion and simplified chemical reaction models used here show that the NO_x catalytic cycle is completely dominant in controlling the local fate of O_3 during the Phase III wake period under most if not all turbulent diffusion regimes to be expected in the lower stratosphere.

The results presented here therefore appear to capture the major part of the potential of SST exhausts for destruction of environmental O_3 while these materials are still rather highly concentrated in intact plumes. However, we hasten to add that these results must be tempered by a clear recognition of uncertainties which only further measurements and experience can reduce. We have attempted to estimate these uncertainties and their possible effects on the validity and interpretation of the analytical results. For one thing, our knowledge of the turbulence structure in the lower stratosphere is still woefully inadequate. For another, the complexity of the chemistry, particularly the reactions involved in photochemical chains affecting O_3 concentrations, still contain enough uncertainty to require sober and skeptical appraisal of any analytical results in which they are included. The present analyses are no exception.

However, with all of these caveats in place, it is still our intention to present the results of our analyses as a contribution to that ultimate management responsibility, namely, to make decisions in the light of incomplete and frequently inaccurate information.

SYMBOLS

a	constant
A	constant
A_i	Lagrangian scale length
b	constant
C_i	concentration of ith chemical species
$\overline{C}_{\beta_c}$	concentration of NO just capable of destroying O_3 at same rate as local production rate of O_3
$C_i'C_j'$	second-order concentration correlation between ith and jth species
$C_i'u_j'$	flux of ith species in jth direction
D	diffusion component of difference between maximum and actual reaction rate in plume
E	chemical efficiency defined by Eq. (62)
E^*	chemical efficiency of NO for destruction of locally produced O_3-defined by Eq. (64)
f_i	frequency distribution
F_{ij}	the jth surface average flux of ith species
g	acceleration due to gravity
k_1, k_2	reaction rate constants
k_y, k_z	eddy diffusivities
L_D	diffusion limitation = D/R^*
L_M	mixedness limitation = M/R^*
M	mixedness component of total reaction rate
N	Brunt-Väisälä frequency = $(g(\partial\overline{T}/\partial z)/\overline{T})^{\frac{1}{2}}$
q	square root of twice the turbulent kinetic energy
R	reaction rate over entire plume
R^*	maximum possible reaction rate
Re	Reynolds number
Ri	Richardson number
Ri_c	critical Richardson number

R_i	correlation coefficient
S	constant; also used for vertical velocity gradient $\partial\bar{u}/\partial z$.
S_i	source term for ith chemical species
S_i^*	sources or sinks of i which are not directly attributable to chemical reactions
t	time
t_d	time required to dilute plume by 10^3
T	duration of Phase III (Eq. (78)) or time between turbulence encounters (Eq. (55))
$\bar{T}$	average absolute temperature
T_o	adiabatic temperature
T'^2	temperature fluctuations
T_R	residence time of plume in lower stratosphere
u	longitudinal velocity
$u_i'u_j'$	second-order correlation of velocity components
UU, VV, WW, UW, UT, WT, TT, QQ, Q	nondimensional representations of $\overline{u'u'}$, $\overline{v'v'}$, $\overline{w'w'}$, $\overline{u'w'}$, $\overline{u'T'}$, $\overline{w'T'}$, $\overline{T'^2}$, q^2 , q as defined by Eqs. (38)
v	lateral velocity
w	vertical velocity
x	longitudinal direction
y	lateral direction
y_c, z_c	coordinates of $\bar{C}_{\beta_c}$ concentration isopleth (Eq. (64))
z	vertical direction
β	constant
$\bar{\epsilon}$	average dissipation of turbulent kinetic energy (Eq. (55))
λ	micro-scale length
Λ_1, Λ_2, Λ_3	scalar length scales
Λ_{2T}, Λ_{2TT}	scalar length scales
Λ_{3P}	scalar length scales
ν	kinematic viscosity of fluid
ξ	dummy variable defined by Eq. (19)
σ_i	standard deviation in ith direction

superscripts

—	mean component
'	fluctuating components

subscripts

chem	depletion rate due to chemical reactions
col	vertical column through plume
e	environment
i	surface average over spherical shell (see Eq. (2))
max	maximum value
o	initial value, or reference to center of plume
v	volume average over spherical shell (see Eq. (2))
α	O_3
β	NO
γ, δ	chemical species other than O_3 and NO
1, 2	species designation

The Implications of Wake-Phase Chemistry and Diffusion in the General Problem of the Environmental Impact of Fleet SST Operations

At this point we may anticipate the results to be developed in the next several sections and note that the major findings of these studies may be summarized as follows:

1. During the Phase III wake period the efficiency of SST-emitted NO for the destruction of environmental O_3 is negligibly small, and

2. The Phase III period can be expected to persist for an elapsed time of the order of weeks to months.

Both of these results depend upon the expectation that turbulent diffusion is weak in the largely stably stratified lower stratosphere. The first result also depends upon simultaneous calculations of the combined effects of diffusive mixing and chemical reactions. The low chemical efficiency of the NO-O_3 reaction is directly attributable to the slow diffusive mixing between the NO plume and the surrounding O_3, and could not be properly anticipated from decoupled solutions of the diffusion

equations and the chemical kinetic equations.

Interesting as these rather novel results are, however, their implications for the overall impact of SST operations on environmental O_3 depend upon a comparison between the duration of the Phase III period and the expected total residence time for SST exhaust materials in the lower stratosphere. Present estimates of this residence time range from a few months to more than a year, but none of these estimates appear to take into account the selective (route) injection of SST exhausts in the middle latitudes of the Northern Hemisphere. (This is the region of selective removal of stratospheric air into the troposphere.) However, without anticipating the results of other analyses of total residence time, we may note that the Phase III chemical inefficiencies constitute a significant effect if the duration of Phase III is a significant fraction of the expected total residence time. For example, if Phase III persists for one month and the expected residence time is three months, the estimate of the depletion of O_3 is reduced to one-half to one-third of previous estimates. Shorter durations of Phase III and/or longer residence times would, of course, reduce these effects to scientifically interesting, but operationally insignificant considerations. At this point, we can only note that neither of these numbers is known within a factor of two (or more) of their true values, and the impact of the Phase III effect cannot be more precisely estimated until this situation is corrected.

THE FRAME OF REFERENCE

In order to establish an appropriate frame of reference for the analyses of the diffusion and chemistry of SST exhausts during the wake phase, we should first consider one of the broader problems to which CIAP must address itself. This may be stated as, "What are the changes in the global equilibrium amount of O_3, given a steady emission of NO from a fleet of SST's flying in the lower stratosphere?" Let α and β denote O_3 and NO, respectively, and C_α and C_β be the local concentrations of these reactants at any particular time. Now consider a spherical shell of the atmosphere, surrounding the globe and defined by the spherical surfaces at heights z_1 and z_2 above the earth's surface. Then the balance equations for α and β within this shell are

$$\left[\frac{dC_\alpha}{dt}\right]_v = \frac{d[C_\alpha]_v}{dt} = [C_\alpha'w']_2 - [C_\alpha'w']_1 - k_1[C_\alpha C_\beta]_v + [S_\alpha]_v \qquad (1)$$

and

$$\left[\frac{dC_\beta}{dt}\right]_v = \frac{d[C_\beta]_v}{dt} = [C_\beta'w']_2 - [C_\beta'w']_1 - k_2[C_\alpha C_\beta]_v + [S_\beta]_v \qquad (2)$$

where $[\ ]_v$ denotes a volume average over the spherical shell and $[\ ]_i$ denotes a surface average over the shell at height i, k_1 and k_2 are the reaction rate constants and S_α and S_β are the source or production rates for α and β within the shell volume. $C_\alpha'w'$ and $C_\beta'w'$ are, of course, the local vertical fluxes of α and β at the designated height. We now assume that the NO_x catalytic cycle operates everywhere to conserve NO and therefore the chemistry term in Equation (2) has a value of 0.

Now consider the case when C_α and C_β are inhomogeneously distributed within the shell and $[C_\alpha]_v$ and $[C_\beta]_v$, the volume averages of C_α and C_β, are constant in time (a steady state assumption for the total amount of O_3 and NO in the shell). Then the local concentrations at any time are defined by

$$C_\alpha = [C_\alpha]_v + C_\alpha' \qquad (3)$$

$$C_\beta = [C_\beta]_v + C_\beta' \qquad (4)$$

and

$$[C_\alpha']_v = [C_\beta']_v = 0 \qquad (5)$$

Then Equations (1) and (2) become

$$\frac{d[C_\alpha]_v}{dt} = F_{\alpha 2} - F_{\alpha 1} - k_1[C_\alpha]_v\,[C_\beta]_v - k_1[C_\alpha'C_\beta']_v + [S_\alpha]_v \qquad (6)$$

and

$$\frac{d[C_\beta]_v}{dt} = F_{\beta 2} - F_{\beta 1} + [S_\beta]_v \qquad (7)$$

where $F_{ij} = [C_i'w']_j$ designates the jth surface average flux of the ith species. We now assume that all of the terms in Equations (6) and (7) are statistically stationary and time average them. Then

$$\frac{d[\overline{C}_\alpha]_v}{dt} = 0 = \overline{F}_{\alpha 2} - \overline{F}_{\alpha 1} - k_1[\overline{C}_\alpha]_v\,[\overline{C}_\beta]_v - k_1[\overline{C_\alpha'C_\beta'}]_v + [\overline{S}_\alpha]_v \qquad (8)$$

and

$$\frac{d[\overline{C}_\beta]_v}{dt} = 0 = \overline{F}_{\beta 2} - \overline{F}_{\beta 1} + [\overline{S}_\beta]_v \qquad (9)$$

Equation (9) simply states the equilibrium amount of NO in the shell is achieved when the average amount injected by the SST's just balances the net flux of NO out of the shell.

However, Equation (8) tells us that the equilibrium amount of O_3 in the shell, as measured by $[\overline{C}_\alpha]_v$, is determined by a balance of the net flux of O_3 into or out of the shell, the local production of O_3, and the degree to which O_3 and NO are mixed within the shell, as well as upon the equilibrium amount of NO in the shell. Rewriting Equation (8), this balance is given by

$$[\overline{C}_\alpha]_v = \frac{1}{k_1[\overline{C}_\beta]_v}\left[\Delta\overline{F}_\alpha - k_1[\overline{C'_\alpha C'_\beta}]_v + [\overline{S}_\alpha]_v\right] \qquad (10)$$

where $\Delta\overline{F}_\alpha$ is the average net flux of O_3 into or out of the shell.

Despite the simplification of the chemistry involved in the derivation of Equation (10), this formulation does clearly reveal the mechanisms which must be considered jointly in determining the overall effect of injection of SST exhausts on the O_3 balance in the lower stratosphere. In particular, it is clear we must determine how any particular mode of emissions of these exhausts, as well as their amount, affect the vertical flux of O_3, $\Delta\overline{F}_\alpha$, the degree of mixedness, $\overline{C'_\alpha C'_\beta}$, and the local production of O_3, $\overline{S}_\alpha$, if the changes in the equilibrium amount of O_3 in any particular atmospheric layer are to be correctly evaluated.

We can note qualitatively (a quantitative treatment follows), that the net flux of O_3, $\Delta\overline{F}_\alpha$, depends upon the vertical gradients of the concentration of O_3 and the nature of the turbulent motions. If $\Delta\overline{F}_\alpha$ is to be evaluated from first principles, we must have a knowledge of how the distribution of NO in the spherical shell has altered the gradients of the O_3 distribution by chemical reaction. The mixedness term $-k_1[\overline{C'_\alpha C'_\beta}]_v$ basically measures the degree to which local fluctuations of the concentrations of O_3 and NO are correlated. As we shall see, this term is produced by the "folding" of anomalous amounts of O_3 and NO without intimate local mixing and is a function of the local gradients of the concentrations of O_3 and NO and of the turbulence field. Estimates of the magnitude of this term therefore also require some knowledge of the distributions of O_3 and NO throughout the shell and the turbulence fields acting on these distributions. This term can be ignored only if we can demonstrate that $[\overline{C'_\alpha C'_\beta}]_v \ll [\overline{C}_\alpha]_v\,[\overline{C}_\beta]_v$, a condition which is not obvious a priori, given the potential

for inhomogeneous mixing of O_3 and NO described previously.

Since the wake phase of SST exhaust dispersion in the lower stratosphere represents the maximum anomaly in NO concentration, an analysis of the balances of NO and O_3 concentrations in these plumes, with accompanying determinations of the diffusive fluxes, diffusive mixing, and chemical reactions which produce these balances, provides the first assessment of these coupled effects and how they might contribute to the global balance of O_3. For this purpose, we adopt a pseudo-Lagrangian frame of reference which moves with the mean motion of a plume segment. In this frame of reference we have removed the large-scale motions of the plume segment (which only control where the segment goes), and have retained only the smaller scale motions, which control the diffusive transport and mixing of the plume segment with its environment. In this frame we also correctly portray the chemical reactions as a function of the local, time dependent, joint concentrations of the reactants. The ensemble averages used in this frame represent the mean and fluctuations over many repetitions of emissions of SST exhausts into turbulence fields which are stochastically determinant. The result of this choice is that each prediction represents an expected value, but is not necessarily appropriate to any single realization of these processes. Since the ultimate interest is in the integration of these results over a sizeable volume and time period, the use of expected value theory is entirely appropriate.

THE ANALYTICAL TOOLS - INVARIANT MODELS OF TURBULENCE, TURBULENT DIFFUSION, AND INHOMOGENEOUS CHEMISTRY

Within the problem orientation and frame of reference described in the previous sections, A.R.A.P. has undertaken the application of the invariant modeling techniques (developed over the past several years by Donaldson and his colleagues) to the problems of coupled diffusion and chemistry in SST wakes. These techniques, and the turbulence, turbulent diffusion, and chemical kinetics models which derive from them, have been described in detail in refs. 5 and 6, and the reader interested in such detail is referred to these reports.

By way of a general description, the invariant modeling techniques depend upon the derivation of dynamical equations for both the first and second-order moments of physical variables which enter into the governing equations for the physical system under study. In any nonlinear system (which is what we are dealing with in turbulence and chemical processes) the dynamical equations for second-order moments generally involve third-order (and sometimes higher) moments of the physical variables and

therefore these equations are not "closed," i.e., we have more unknowns than equations. At this point one has the option of deriving the dynamical equations for the higher-order moments, but these, of course, produce still higher moments and do not provide closure. In addition the number of equations which must be solved simultaneously proliferate quite markedly as one goes to higher and higher moments.

Donaldson's approach to this closure problem was to establish rules of invariance for finding approximate values of the third-order moments in terms of the first- and second-order moments of the physical variables. In particular, the coefficients which enter into the approximate functional relationships between the third-order and the lower-order moments were to be invariant for any change of the coordinate system. In addition, the rules of invariance required that all tensor symmetries be preserved and that all conservation laws be observed.

Invariant modeling is therefore a second-order closure technique, analogous to first-order closure techniques (in which second-order moments are modeled as functions of first-order moments), but has the distinct advantage of retaining prediction equations for the second-order moments explicitly. Terms such as $\overline{C'_\alpha w'}$ and $\overline{C'_\alpha C'_\beta}$ discussed in the previous section are now explicit variables in the models and can be examined specifically in the solutions of the models. These models are, of course, still approximate (as any model of nonlinear systems must be), and the coefficients which enter into the closure relationships must still be evaluated empirically. The rule of invariance is particularly powerful here since these coefficients may be evaluated in one coordinate system and then be applied to another. (For an example of the power of this technique see ref. 8 where coefficients derived from laboratory measurements were used to establish the Monin - Obukhov similarity functions for atmospheric boundary layer flows.) However, as noted throughout this report, the values of these coefficients for lower stratospheric flow are not rigorously established, and the results of model calculations are uncertain within this degree of ignorance. Since this same uncertainty afflicts all models, only appropriate measurements can overcome this handicap.

Finally, a distinct advantage of second-order closure models over mean-value (first-order closure) models is that the former are inherently time dependent and can therefore be used to predict the response of the modeled system to time dependent forcing functions. In nonsteady turbulence systems, of which there is some evidence the lower stratosphere is one, this property permits consistent analyses without grossly arbitrary assumptions regarding such parameters as the effective eddy diffusivity.

The General Diffusion and Chemistry Model

In approaching the problem of modeling the diffusion and chemical reaction of two chemical species α and β, we begin with the equations for mass continuity of each species.

$$\frac{\partial C_\alpha}{\partial t} + u\frac{\partial C_\alpha}{\partial x} + v\frac{\partial C_\alpha}{\partial y} + w\frac{\partial C_\alpha}{\partial z} = \nu_o\left(\frac{\partial^2 C_\alpha}{\partial x^2} + \frac{\partial^2 C_\alpha}{\partial y^2} + \frac{\partial^2 C_\alpha}{\partial z^2}\right) + S_\alpha \tag{11}$$

and

$$\frac{\partial C_\beta}{\partial t} + u\frac{\partial C_\beta}{\partial x} + v\frac{\partial C_\beta}{\partial y} + w\frac{\partial C_\beta}{\partial z} = \nu_o\left(\frac{\partial^2 C_\beta}{\partial x^2} + \frac{\partial^2 C_\beta}{\partial y^2} + \frac{\partial^2 C_\beta}{\partial z^2}\right) + S_\beta \tag{12}$$

where u, v, and w are the instantaneous components of motion along x, y, and z, respectively, ν_o is the kinematic viscosity of the fluid, and S_α and S_β are any local sources or sinks of the α and β species, including chemical alteration. We separate out the chemical alteration part of S_α and S_β by noting from the reaction

$$\alpha + \beta \rightarrow \gamma + \delta \tag{13}$$

$$\frac{\partial C_\alpha}{\partial t} + \frac{\partial C_\beta}{\partial t} = \frac{\partial C_\gamma}{\partial t} + \frac{\partial C_\delta}{\partial t} \tag{14}$$

and writing the chemical kinetics equations

$$\left(\frac{\partial C_\alpha}{\partial t}\right)_{chem} = -k_1 C_\alpha C_\beta \tag{15}$$

and

$$\left(\frac{\partial C_\beta}{\partial t}\right)_{chem} = -k_2 C_\alpha C_\beta \tag{16}$$

Then, if we follow only α and β, we have

$$S_\alpha = S_\alpha^* + \left(\frac{\partial C_\alpha}{\partial t}\right)_{chem} \tag{17}$$

and

$$S_\beta = S_\beta^* + \left(\frac{\partial C_\beta}{\partial t}\right)_{chem} \tag{18}$$

where S^* now includes all sources and sinks not attributable to the chemical alteration of α and β according to Equation (13).

We now assume that an ensemble average of the physical variables in the frame of reference just described is statistically stationary and we can write any of these variables in the form

$$\xi = \overline{\xi} + \xi' \tag{19}$$

where $\xi = u, v, w, C_\alpha$, and C_β. Substituting Equations (17), (18) and (19) into Equations (11) and (12), time averaging and rearranging terms gives

$$\frac{\partial \overline{C}_\alpha}{\partial t} + \overline{u}\frac{\partial \overline{C}_\alpha}{\partial x} + \overline{v}\frac{\partial \overline{C}_\alpha}{\partial y} + \overline{w}\frac{\partial \overline{C}_\alpha}{\partial z} = \nu_o\left(\frac{\partial^2 \overline{C}_\alpha}{\partial x^2} + \frac{\partial^2 \overline{C}_\alpha}{\partial y^2} + \frac{\partial^2 \overline{C}_\alpha}{\partial z^2}\right)$$

$$+ \frac{\partial}{\partial x}\left(\overline{C_\alpha' u'}\right) + \frac{\partial}{\partial y}\left(\overline{C_\alpha' v'}\right) + \frac{\partial}{\partial z}\left(\overline{C_\alpha' w'}\right)$$

$$- k_1\left(\overline{C}_\alpha \overline{C}_\beta + \overline{C_\alpha' C_\beta'}\right) + \overline{S}_\alpha^* \tag{20}$$

and

$$\frac{\partial \overline{C}_\beta}{\partial t} + \overline{u}\frac{\partial \overline{C}_\beta}{\partial x} + \overline{v}\frac{\partial \overline{C}_\beta}{\partial y} + \overline{w}\frac{\partial \overline{C}_\beta}{\partial z} = \nu_o\left(\frac{\partial^2 \overline{C}_\beta}{\partial x^2} + \frac{\partial^2 \overline{C}_\beta}{\partial y^2} + \frac{\partial^2 \overline{C}_\beta}{\partial z^2}\right)$$

$$+ \frac{\partial}{\partial x}\left(\overline{C_\beta' u'}\right) + \frac{\partial}{\partial y}\left(\overline{C_\beta' v'}\right) + \frac{\partial}{\partial z}\left(\overline{C_\beta' w'}\right)$$

$$- k_2\left(\overline{C}_\alpha \overline{C}_\beta + \overline{C_\alpha' C_\beta'}\right) + \overline{S}_\beta^* \tag{21}$$

For convenience we now assume a statistically steady state, so that $\partial/\partial t = 0$, and a coordinate system with x oriented along the direction of mean flow so that $\overline{v} = \overline{w} = 0$. With these assumptions we have two equations and the following unknowns:

First-order: $\overline{c}_\alpha$ and $\overline{c}_\beta$

Second-order: $\overline{c'_\alpha u'}$, $\overline{c'_\alpha v'}$, $\overline{c'_\alpha w'}$, $\overline{c'_\beta u'}$, $\overline{c'_\beta v'}$, $\overline{c'_\beta w'}$ and

$$\overline{c'_\alpha c'_\beta}$$

if $\overline{u}$, ν_o , k_1 , k_2 , $\overline{S}^*_\alpha$, and $\overline{S}^*_\beta$ can be independently specified. Since we have seven more unknowns than equations (all second-order unknowns) we need seven equations for these second-order correlations. However, Equations (20) and (21) are the ones we wish to solve for conditions appropriate to the Phase III period of SST wakes.

The Sub-Models

In developing the prediction system which permits approximate solutions of Equations (20) and (21) three invariant sub-models have been constructed. The first, the turbulence sub-model, provides the prediction of the local values of turbulent motions, $\overline{u'^2}$, $\overline{v'^2}$, and $\overline{w'^2}$ and temperature fluctuations, $\overline{T'^2}$, and their various moments, e.g., $\overline{w'T'}$, given the input values for the average wind velocity and the average temperature as a function of height z . This sub-model is described in some detail in the next section.

The second sub-model accepts the mean and turbulent values of the fields of motion and temperature generated by the first sub-model, combines these inputs with the initial distribution of a conservative tracer (gaseous or aerosol) material and predicts the three-dimensional diffusion of the tracer material in this field of turbulence. (These are essentially solutions of Equations (20) or (21) without the chemistry term - $k(\overline{c}_\alpha\overline{c}_\beta + \overline{c'_\alpha c'_\beta})$.) The input distribution of the concentration of the tracer material may be any arbitrary source geometry (within the constraints on spatial slopes and curvatures imposed by the numerical solution techniques). For any individual SST plume this model can therefore be started at any stage of the plume growth if the distribution of tracer concentration at that stage is known. This model may be used to predict the growth and dilution of chemically nonreactive exhaust materials, but its primary utility in the present application has been through its coupling with the chemistry sub-model.

The chemistry sub-model, which was partially developed under CIAP-related programs (see ref. 6), is basically designed to predict chemical reaction rates for a binary, isothermal reaction system in which the reactants are inhomogeneously distributed. The sub-model includes only the chemical kinetics of this system,

i.e., any mixing processes are excluded. In this form, the model accepts any appropriate combination of the means and second-order correlations of the concentrations of the reactants and predicts the reaction rates and the depletion of each species until the reaction proceeds to exhaustion of either or both of the reactants in each elemental volume of the reactor. Since very few, if any, data on chemical reactions at the time and space resolution required are available, this sub-model has been validated against exact solutions of the chemical kinetics equations. This procedure was particularly important in the development and testing of the closure approximations for the third-order moments of the concentration fluctuations.

Probably the most valuable aspect of this sub-model development has been a more rigorous definition of the circumstances under which the effects of inhomogeneous mixing of reactants significantly retards or enhances their reaction rate. These conditions are described in ref. 7, but may be summarized by the observation that reaction rates can depart drastically from those predicted by mean value chemical kinetics when the product of the variance-to-mean-squared ratios for the reactants' concentrations exceed one. This situation is readily realized when reactants are emitted at relatively high concentrations from multiple sources, which is, of course, the case for multiple SST flights.

The Coupled Invariant Chemistry and Diffusion Model

With the successful development of the sub-models described above, it has been possible to combine them into an initial version of a coupled turbulent diffusion and inhomogeneous chemistry model. The presently operating version of the coupled model and its development are described in ref. 6. For several reasons, the primary one being sheer computational complexity, the initial model was developed for the following conditions:

1. Horizontal straight-line flow with $\bar{u}$ as a function of height only.

2. Horizontally homogeneous turbulence.

3. No coupling between reactant densities or reactions and the turbulence or flow fields. (Density and thermal effects are negligible.)

4. Binary and isothermal chemical reactions.

5. Two-dimensional (z and t) coupled diffusion and chemistry. (Lateral and longitudinal diffusion negligible in comparison with the vertical component.)

Although these conditions may appear restrictive, they capture a large part of the realism of the SST wake features which we wish to analyze and, even though simplified, they do permit a first critical analysis of the interaction of diffusion and chemistry in a turbulent, nonhomogeneous system.

The first three of the above conditions permit us to decouple the turbulence sub-model, since there is no feedback from either the presence of the reactants or their chemical reaction into the field of turbulence. This is not the case for the turbulent diffusion and chemistry sub-models, however, since in general there are intimate interactions between the diffusive mixing and transport of the reactants and their chemical reaction rates. As will be shown later, several of the important results of this interaction cannot be captured by decoupled solutions of the diffusion and chemistry equations. The coupled diffusion and chemistry model constitutes the fourth invariant sub-model, sub-model in the sense that it depends upon the turbulence sub-model as one of its inputs.

In addition to the turbulence field input, the diffusion/chemistry model requires an initial specification of the spatial (vertical) distributions of the concentration of the reactants, any initial second-order moments of these concentrations, and the reaction rate constants. Since the model calculates the consistent set of second-order moments for both diffusion and chemical reactions out of the production, diffusion, and dissipation rates for these quantities, they are normally set equal to zero initially and their time history is then reckoned from the time the model brings them into equilibrium with all of the input conditions. From that time on the basic outputs of the model are the time histories of the distributions of the reactants and the separate rates of diffusion and chemical depletion which produce these distributions. These outputs may be manipulated to produce any measure of these processes desired, e.g., the central value and variance of the concentration distributions, total chemical depletion, local diffusive flux rates, etc.

ESTIMATES OF DIFFUSIVE TURBULENCE IN THE LOWER STRATOSPHERE

Any logical assessment of the behavior of SST exhaust plumes in the lower stratosphere must begin with a specification of the characteristics of the fields of turbulence in which these plumes will be embedded. As a minimum, these turbulent motions will control the rate at which exhaust products are diluted by and mingle with the environmental constituents and are therefore prime agents in determining the fate of these materials. Because of

the fragmentary data on turbulence in the lower stratosphere and in view of its importance to any attempt to model the diffusion of materials, we have conducted an extensive study of the possible modes of turbulent motions, including continuous as well as discontinuous turbulence generation in the lower stratosphere; these results are reported extensively in this section, as a convenience to other modelers who may not be familiar with these data.

The evidence regarding turbulence in the lower stratosphere is not only fragmentary; it is also somewhat contradictory. By far the most extensive measurements have been made from aircraft flying in the appropriate altitude zone (cf. ref. 9). From literally thousands of hours of flight time (using only instrumented flight observations and ignoring pilot reports) it appears detectable turbulence occurs in this height zone about one to five per cent of the time, the lower frequency associating with ocean and flat-land surfaces and the higher frequency with tall mountain areas. These data suggest that a very large fraction of the lower stratosphere is not turbulent. However, this inference must be drawn with caution, since the lower limit of detectability of turbulence for the instrumentation used on these flights was about 15 cm/sec (rms gust velocities). Turbulence levels below this value are still quite effective as diffusion agents.

Somewhat supportive to the concept of very small turbulent motions (and even laminar flow) in the lower stratosphere are the preponderance of upper air soundings which show combinations of wind shear and temperature lapse rates much in excess of the critical Richardson number. (An example is provided later.) These data are now extensive for most of the globe and at least require the postulation of turbulence generation mechanisms other than steady wind shear and buoyancy if a continuous level of small-scale turbulence is to be sustained in the lower stratosphere.

Offsetting the aircraft and sounding data, however, is a growing body of observations of the motions and at least visual growth of visible smoke puffs and trails (cf. refs. 10 and 11). Although still far less extensive than aircraft and sounding data (and perhaps somewhat biased by analytic selectivity), these visual smoke observations almost universally indicate small-scale shears and diffusion, and not laminar flow.

Since direct observations of the turbulence are apparently not yet adequate to a decision as to how extensive and intensive stratospheric turbulence is, we have utilized the invariant turbulence model to predict turbulence levels and decay for the whole range of Richardson numbers which might occur, and have then investigated the effects of both continuous and discontinuous turbulence on the behavior of SST exhaust plumes. Perhaps not too surprisingly the net effects are not very different; the end results are arrived at in about the same length of time, although

by very different time histories.

The Turbulence Model

If we consider the motion in the stratosphere to be governed by the equations for an incompressible, two-dimensional, turbulent free shear layer, then the equations which define the turbulent flow field may be written in the following form (ref. 5). In these equations, u is the free stream velocity in the x direction and z is the direction normal to x in which large gradients in u exist.

Turbulent Energy Components $(\overline{u'^2}, \overline{v'^2}, \overline{w'^2})$

$$\frac{D}{Dt}(\overline{u'^2}) = -2\,\overline{u'w'}\,\frac{\partial \bar{u}}{\partial z} + \frac{\partial}{\partial z}\left(\Lambda_2 q \frac{\partial}{\partial z}\overline{u'^2}\right)$$

$$- \frac{q}{\Lambda_1}\left(\overline{u'^2} - \frac{q^2}{3}\right) + \frac{\nu}{Re}\frac{\partial^2}{\partial z^2}(\overline{u'^2})$$

$$- \frac{2\nu\beta}{Re\lambda^2}\overline{u'^2} - \frac{2\nu(1-\beta)}{Re}\left\{\frac{q^2}{3\lambda^2} + \frac{a}{\Lambda_1^2}\left(\overline{u'^2} - \frac{q^2}{3}\right)\right\} \quad (22)$$

$$\frac{D}{Dt}(\overline{v'^2}) = \frac{\partial}{\partial z}\left(\Lambda_2 q \frac{\partial}{\partial z}\overline{v'^2}\right) - \frac{q}{\Lambda_1}\left(\overline{v'^2} - \frac{q^2}{3}\right)$$

$$+ \frac{\nu}{Re}\frac{\partial^2}{\partial z^2}(\overline{v'^2}) - \frac{2\nu\beta}{Re\lambda^2}\overline{v'^2} - \frac{2\nu(1-\beta)}{Re}$$

$$\left\{\frac{q^2}{3\lambda^2} + \frac{a}{\Lambda_1^2}\left(\overline{v'^2} - \frac{q^2}{3}\right)\right\} \quad (23)$$

$$\frac{D}{Dt}\left(\overline{w'^2}\right) = 3\frac{\partial}{\partial z}\left(\Lambda_2 q \frac{\partial}{\partial z}\overline{w'^2}\right) + 2\frac{\partial}{\partial z}\left(\Lambda_3 q \frac{\partial}{\partial z}\overline{w'^2}\right)$$

$$- \frac{q}{\Lambda_1}\left(\overline{w'^2} - \frac{q^2}{3}\right) + \frac{\nu}{Re}\frac{\partial^2}{\partial z^2}\left(\overline{w'^2}\right) + \frac{2g}{T_o}\overline{w'T'}$$

$$- \frac{2\nu\beta}{Re\lambda^2}\overline{w'^2} - \frac{2\nu(1-\beta)}{Re}\left\{\frac{q^2}{3\lambda^2} + \frac{a}{\Lambda_1^2}\left(\overline{w'^2} - \frac{q^2}{3}\right)\right\} \qquad (24)$$

Reynolds Stress $(\overline{u'w'})$

$$\frac{D}{Dt}\left(\overline{u'w'}\right) = -\overline{w'^2}\frac{\partial\overline{u}}{\partial z} + 2\frac{\partial}{\partial z}\left(\Lambda_2 q \frac{\partial}{\partial z}\overline{u'w'}\right) + 3\frac{\partial}{\partial z}\left(\Lambda_3 q \frac{\partial}{\partial z}\overline{u'w'}\right)$$

$$- \frac{q}{\Lambda_1}\overline{u'w'} + \frac{\nu}{Re}\frac{\partial^2}{\partial z^2}\overline{u'w'} + \frac{g}{T_o}\overline{u'T'} - \frac{2\nu\beta}{Re\lambda^2}\overline{u'w'}$$

$$- \frac{2\nu(1-\beta)}{Re}\frac{a}{\Lambda_1^2}\overline{u'w'} \qquad (25)$$

Heat Fluxes $(\overline{u'T'}, \overline{w'T'})$

$$\frac{D}{Dt}\left(\overline{u'T'}\right) = -\overline{u'w'}\frac{\partial\overline{T}}{\partial z} - \overline{w'T'}\frac{\partial\overline{u}}{\partial z} + \frac{\partial}{\partial z}\left(\Lambda_{2T} q \frac{\partial}{\partial z}\overline{u'T'}\right)$$

$$+ \frac{\nu}{Re}\frac{\partial^2}{\partial z^2}\overline{u'T'} - \frac{qA}{\Lambda_1}\overline{u'T'} \qquad (26)$$

$$\frac{D}{Dt}\left(\overline{w'T'}\right) = -\overline{w'^2}\frac{\partial\overline{T}}{\partial z} + 2\frac{\partial}{\partial z}\left(\Lambda_{2T}q\frac{\partial}{\partial z}\overline{w'T'}\right)$$

$$+\frac{\partial}{\partial z}\left(\Lambda_{3P}q\frac{\partial}{\partial z}\overline{w'T'}\right) + \frac{\nu}{Re}\frac{\partial^2}{\partial z^2}\overline{w'T'}$$

$$-\frac{qA}{\Lambda_1}\overline{w'T'} + \frac{g}{T_o}\overline{T'^2} \qquad (27)$$

Temperature Variance $(\overline{T'^2})$

$$\frac{D}{Dt}\left(\overline{T'^2}\right) = -2\,\overline{w'T'}\frac{\partial T}{\partial z} + \frac{\partial}{\partial z}\left(\Lambda_{2TT}q\frac{\partial}{\partial z}\overline{T'^2}\right)$$

$$+\frac{\nu}{Re}\frac{\partial^2}{\partial x^2}\overline{T'^2} - \frac{2\nu S}{Re}\frac{\overline{T'^2}}{\lambda^2} \qquad (28)$$

The micro-scale length (λ) is related to the macro-scale length (Λ_1) by the relation

$$\lambda = \frac{\Lambda_1}{\sqrt{a + b\,Re}} \qquad (29)$$

If we specify the vertical shear $(\partial\overline{u}/\partial z)$ and stability $(\partial\overline{T}/\partial z)$, then Equations (22) to (28) can be solved simultaneously for the turbulence field at any time t. The model parameters which provide the best agreement with data for the wide range of flow applications (jets, wakes, boundary layers, vortices) presently under investigation at A.R.A.P. are:

$$a = 2.5$$

$$b = 0.125$$

$$\beta = 0.$$

$$A = 0.75$$

$$S = 1.8$$

$$\Lambda_3 = \Lambda_{3P} = -0.3\Lambda_1$$

$$\Lambda_2 = \Lambda_{2T} = \Lambda_{2TT} = 0.3\Lambda_1$$

Λ_1 = a parameter for this investigation

Analyses of Steady and Continuous Turbulence in the Stratosphere

If the wind shear and stability in the stratosphere are such that the Richardson number ($Ri = g(\partial\overline{T}/\partial z)/T_0(\partial\overline{u}/\partial z)^2$) is less than the critical value*, then Equations (22) to (28) yield a steady-state solution for the turbulent flow field. In this section, we examine the effects of 1) wind shear, 2) stability, 3) macro-length scale, 4) initial turbulent energy and 5) initial momentum and energy fluxes on the steady-state turbulent fluctuations and on the time required to reach steady state. First, we illustrate some typical results using the numerical model described by Equations (22) to (28) and then demonstrate the feasibility of using a simplified model to estimate the equilibrium turbulence field without resorting to the complete set of partial differential equations.

For purposes of this analysis, we will assume that the shear layer has a height of 2 km and that the scale length, Λ_1, is constant with time. Typical results illustrating the effects of wind shear, stability and scale length are shown in Figs. 1 to 3. For each calculation, the initial turbulent energy ($\frac{1}{2} q_0^2$) is 0.4 m^2/sec^2 and the turbulence is isotropic. In addition, the initial Reynolds stress and heat fluxes are 0. Although the initial profile assumptions, by definition, have no effect on the steady-state solutions, their influence on the transient behavior of the turbulence is not known a priori. Figures 4 and 5 will be used to demonstrate these effects.

Figure 1 illustrates the effect of wind shear on the vertical velocity fluctuations for fixed stability ($d\overline{T}/dz$ = 1 deg/km) and scale length (Λ_1 = 15 m). The strongly-sheared layer (s = 0.05 sec^{-1}) corresponds to a Richardson number of 0.02; the least sheared layer s = .009 sec^{-1} corresponds to the critical Richardson number of 0.55 and, therefore, does not yield a steady-state solution with time**.

*It can be demonstrated that the critical Richardson number is 0.55 for the model parameters given in the previous section rather than the generally accepted value of 0.25.

**A later section deals with the solution when $Ri > Ri_{crit}$.

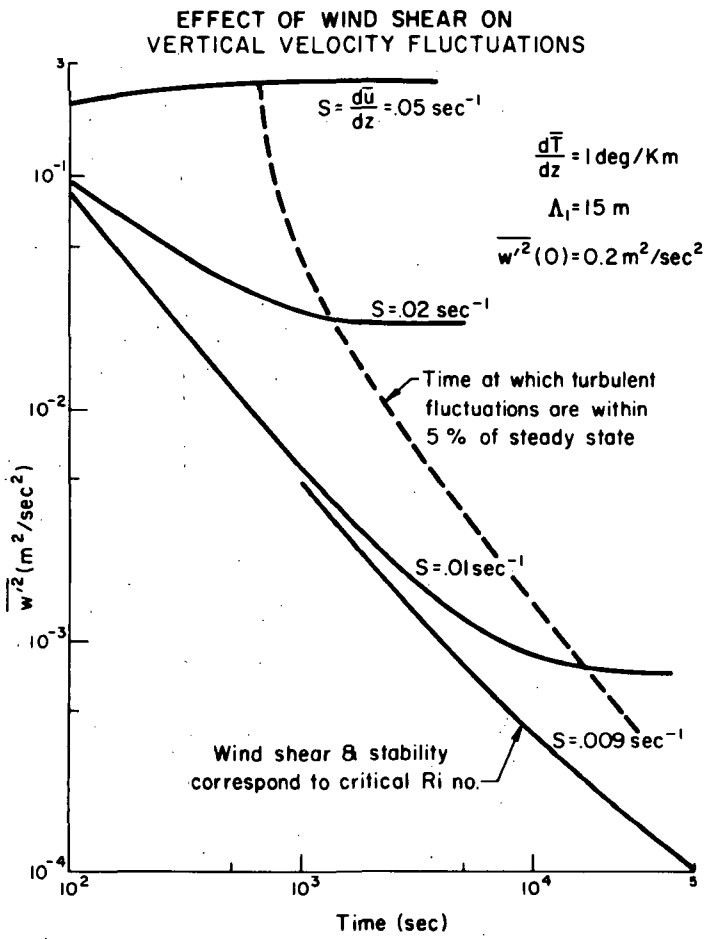

Figure 1. Invariant model calculations of the dependence of vertical turbulence intensity on wind shear.

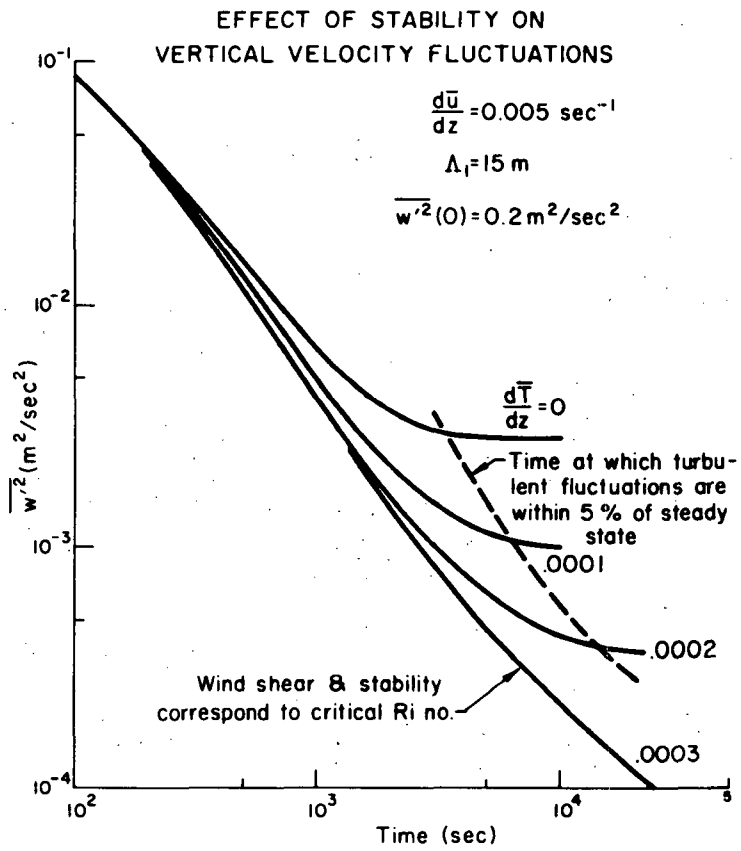

Figure 2. Invariant model calculations of the dependence of vertical turbulence intensity on temperature lapse rate.

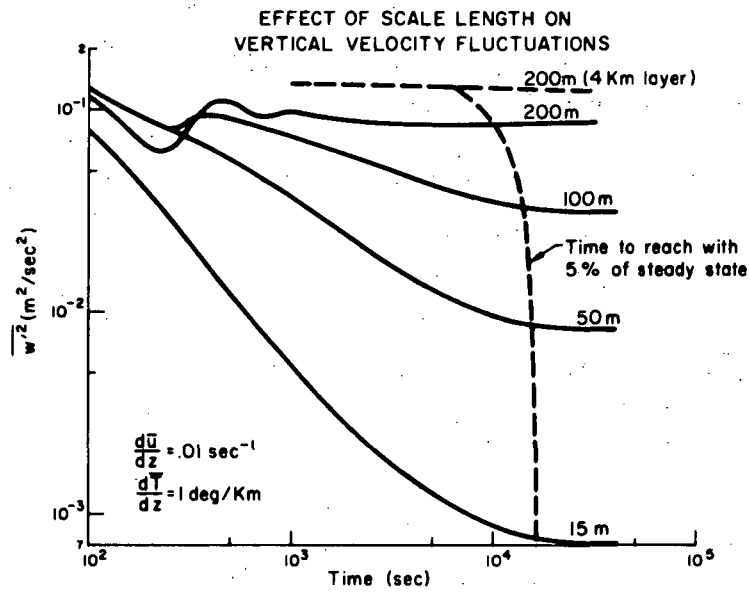

Figure 3. The dependence of vertical turbulence intensity on the macro-scale length, Λ_1.

The strong influence of wind shear on the velocity fluctuations is evident. A five-fold decrease in shear from .05 to .01 sec^{-1} results in a decrease in turbulent energy of nearly two orders of magnitude.

The effect of wind shear on the remaining turbulent fluctuations is summarized in Table 1.

TABLE 1

Effect of Wind Shear on Turbulent Fluctuations $d\bar{T}/dz$ = 1 deg/km , Λ_1 = 15 m			
Turbulent Fluctuation	Wind Shear (sec^{-1})		
	.05	.02	.01
$\overline{u'^2}$ (m^2/sec^2)	.53	$.58 \times 10^{-1}$	$.24 \times 10^{-2}$
$\overline{v'^2}$ (m^2/sec^2)	.26	$.27 \times 10^{-1}$	$.10 \times 10^{-2}$
$\overline{w'^2}$ (m^2/sec^2)	.25	$.23 \times 10^{-1}$	$.73 \times 10^{-3}$
$\overline{u'w'}$ (m^2/sec^2)	-.18	$-.17 \times 10^{-1}$	$-.29 \times 10^{-3}$
$\overline{u'T'}$ (m-°C/sec)	$.82 \times 10^{-2}$	$.21 \times 10^{-2}$	$.14 \times 10^{-3}$
$\overline{w'T'}$ (m-°C/sec)	$-.47 \times 10^{-2}$	$-.92 \times 10^{-3}$	$-.15 \times 10^{-4}$
$\overline{T'^2}$ ($°C^2$)	$.31 \times 10^{-3}$	$.19 \times 10^{-3}$	$.15 \times 10^{-4}$
Ri	.02	.11	.45

Note that there are significant changes for all of the fluctuations, although the velocity fluctuations are more strongly influenced by the wind shear than are the temperature fluctuations. Also note that in a shear flow, for conditions of neutral stability, the components of the turbulent kinetic energy are given by $\overline{v'^2} = \overline{w'^2} = \frac{1}{2}\overline{u'^2}$ and this relationship becomes more anisotropic with decreasing shear.

The dashed curve superimposed on Fig. 1 shows the time required to reach within 5% of the steady-state value. Steady-state is achieved within 10 minutes for the strongly-sheared layer, and within approximately 4.5 hours for $s = .01\ sec^{-1}$. For shears between $.01\ sec^{-1}$ and $.009\ sec^{-1}$, the decay time grows exponentially to infinity. That is to say, there is no steady-state solution for a wind shear of $.009\ sec^{-1}$ (when the temperature gradient is 1 deg/km).

Figure 2 illustrates the effect of stability on the vertical velocity fluctuations. Stable potential temperature gradients between 0(Ri = 0) and 0.0003 (Ri = 0.55) are shown for fixed wind shear ($s = .005\ sec^{-1}$) and scale length ($\Lambda_1 = 15$ m) . It is evident that increased stability results in a significant reduction of the steady-state turbulent energy. Changes in the other turbulent fluctuations are summarized in Table 2.

TABLE 2

Effect of Stability on Turbulent Fluctuations
$d\bar{u}/dz = .005\ sec^{-1}$, $\Lambda_1 = 15$ m

Turbulent Fluctuation	Stability (deg/m)		
	0	.0001	.0002
$\overline{u'^2}$ (m^2/sec^2)	$.56 \times 10^{-2}$	$.27 \times 10^{-2}$	$.12 \times 10^{-2}$
$\overline{v'^2}$ (m^2/sec^2)	$.28 \times 10^{-2}$	$.12 \times 10^{-2}$	$.51 \times 10^{-3}$
$\overline{w'^2}$ (m^2/sec^2)	$.28 \times 10^{-2}$	$.10 \times 10^{-2}$	$.37 \times 10^{-3}$
$\overline{u'w'}$ (m^2/sec^2)	$-.20 \times 10^{-2}$	$-.70 \times 10^{-3}$	$-.20 \times 10^{-3}$
$\overline{u'T'}$ (m-°C/sec)	0	$.38 \times 10^{-4}$	$.28 \times 10^{-4}$
$\overline{w'T'}$ (m-°C/sec)	0	$-.30 \times 10^{-4}$	$-.48 \times 10^{-5}$
$\overline{T'^2}$ ($°C^2$)	0	$.12 \times 10^{-5}$	$.14 \times 10^{-5}$
Ri	0	.18	.36

Although the Richardson number variation is similar for Tables 1 and 2, the wind shear has a much larger effect on the turbulent flow field than does the stability. For example, the Reynolds stress ($\overline{u'w'}$) has decreased by a factor of ten due to stability and by a factor of 1000 due to wind shear. This comparison suggests that wind shear is the dominant parameter for the turbulent stratosphere.

One other point should be noted in Table 2, namely, the increasing anisotropy with increasing stability. For the neutral stratosphere ($d\bar{T}/dz = 0$), $\overline{v'^2} = \overline{w'^2} = \frac{1}{2}\overline{u'^2}$; for the more stable stratosphere ($d\bar{T}/dz = .0003$), $\overline{w'^2} = .31\ \overline{u'^2}$ and $\overline{v'^2} = 1.4\ \overline{w'^2}$. In essence, the stability suppresses the vertical velocity fluctuations.

Stability has approximately the same effect on the time to reach steady-state as does wind shear. The dashed curve on Fig. 2 shows that the equilibration time is between 1 and 4 hours and increasing with stability.

The computations described above were based on a constant scale length of 15 m. Many investigations, including our own current estimates, indicate that the scale is probably of the

order of 100-200 meters or more. If this is indeed the case, then the turbulent fluctuations can be considerably higher than for the 15 m scale length.

In order to illustrate the effect of scale length, we have recomputed the turbulent flow field for one of the above cases (i.e., $d\bar{u}/dz = .01$ sec^{-1} , $d\bar{T}/dz = .001$ deg/m , and Ri = .45) with scale lengths of 50, 100, and 200 m. The results are illustrated in Fig. 3.

Before discussing these results, we should note two aspects of this figure. First, two curves are presented for the 200 m case. The solid line is for a 2 km layer, which is the thickness used for the smaller scale lengths. The broken-dashed line is for a 4 km layer. It was found that the 2 km thickness suppressed the turbulent fluctuations for scale lengths in excess of 100 m because relatively steep gradients of the turbulent fluctuations are established in order to satisfy the zero turbulence boundary condition. This increases diffusion from the center of the layer and, hence, lowers turbulent fluctuations. Since these decreases are not the result of scale length, we decided to increase the layer thickness to 4 km. For this thickness, diffusion from the center of the layer is relatively unaffected by the boundary conditions. Therefore, the difference between the dashed curve and the three lower curves is solely the result of varying the scale length. In essence, one may think of Fig. 3 as showing the effect of scale length for a 4 km layer since the 15, 50 and 100 m curves are unchanged for the thicker layer. We will use the 4 km results in the following discussion.

The second point to note is that damped oscillations occur for the first 15 minutes as the momentum and energy fluxes (which are initially zero) seek to adjust to the turbulent energies. Such oscillations are not numerical anomalies but rather an accurate representation of the physical process which would occur subsequent to the assumed initial conditions.

The most important point to be gleaned from Fig. 3 is that the velocity fluctuations are proportional to the square of the scale length. This is not too surprising in view of the form of Eqs. (22) to (28). Steady-state represents an unchanging balance of turbulent production, diffusion and dissipation. The dissipation is inversely proportional to $Re \cdot \lambda^2$ which, for large Reynolds number, is proportional to Λ^2 . Thus, larger Λ means less dissipation and, hence, more turbulence. Our results show that since the turbulence is dominated by the dissipation term, the diffusion terms are relatively unimportant for the steady-state solution. We will return to this point at the end of this section when we discuss superequilibrium.

The scaling law is not limited to velocity fluctuations only. Table 3 summarizes the effect of scale length on all the turbulent fluctuations. Without exception, the fluctuations are proportional to Λ_1^2 .

TABLE 3

Effect of Scale Length on Turbulent Fluctuations
$d\bar{u}/dz = .01\ sec^{-1}$ $d\bar{T}/dz = 1$ deg/km

Turbulent Fluctuation	Scale Length (Λ_1) m			
	15	50	100	200
$\overline{u'^2}$ (m^2/sec^2)	$.24 \times 10^{-2}$	$.26 \times 10^{-1}$	.10	.41
$\overline{v'^2}$ (m^2/sec^2)	$.10 \times 10^{-2}$	$.11 \times 10^{-1}$	$.44 \times 10^{-1}$	.18
$\overline{w'^2}$ (m^2/sec^2)	$.73 \times 10^{-3}$	$.82 \times 10^{-2}$	$.31 \times 10^{-1}$	.12
$\overline{u'w'}$ (m^2/sec^2)	$-.29 \times 10^{-3}$	$-.32 \times 10^{-2}$	$-.12 \times 10^{-1}$	$-.49 \times 10^{-1}$
$\overline{u'T'}$ (m-°C/sec)	$.14 \times 10^{-3}$	$.15 \times 10^{-2}$	$.59 \times 10^{-2}$	$.23 \times 10^{-1}$
$\overline{w'T'}$ (m-°C/sec)	$-.15 \times 10^{-4}$	$-.16 \times 10^{-3}$	$-.63 \times 10^{-3}$	$-.25 \times 10^{-2}$
$\overline{T'^2}$ ($°C^2$)	$.15 \times 10^{-4}$	$.17 \times 10^{-3}$	$.66 \times 10^{-3}$	$.26 \times 10^{-2}$

The final point to note from Fig. 3 is that the scale length has a minor influence on the time required to reach steady state. Equilibration occurs in less than 4 hours.

Each of the computations described above is based on the same initial conditions. In particular, the initial turbulent kinetic energy is 0.4 m^2/sec^2, the turbulence is isotropic and the momentum and heat fluxes are zero. In order to illustrate the effect of initial conditions on the turbulence, we varied both the initial kinetic energy and initial fluxes.

Figure 4 illustrates the transient behavior of $\overline{w'^2}$ for three different energy levels which vary over a span of two orders of magnitude. In each instance, the identical steady-state solution is reached in approximately 4 hours. During the first 4 hours, however, the transient adjustment is strongly influenced by the initial energy. The highly energetic layer decays smoothly to the equilibrium level, while the least energetic layer undergoes rapid readjustment in the first 10 seconds as the Reynolds stresses are generated and then decays most rapidly to the equilibrium state.

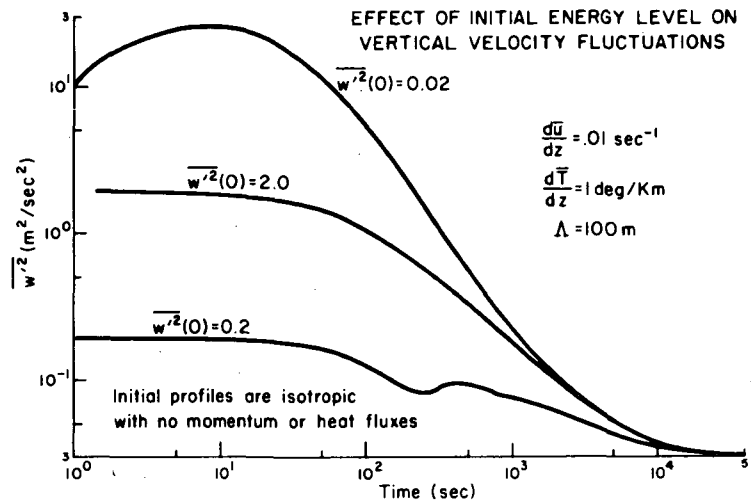

Figure 4. The dependence of vertical turbulence intensity upon initial conditions chosen for invariant model simulations.

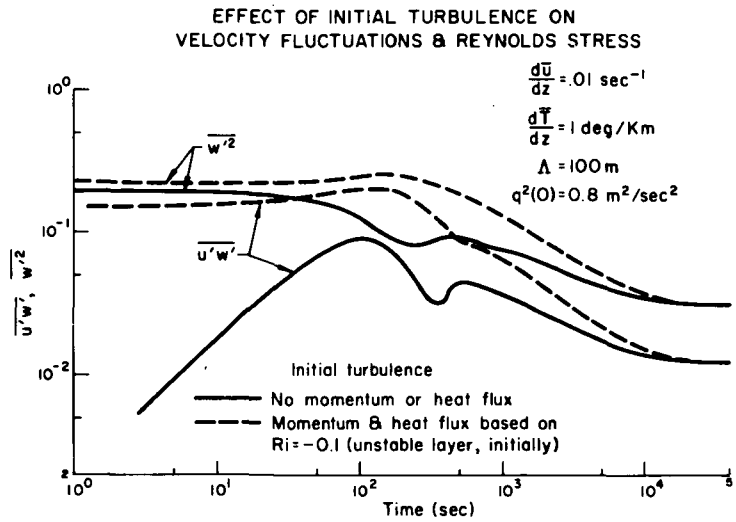

Figure 5. Dependence of vertical turbulence and shear stress on initial conditions chosen for shear stress and vertical heat flux.

In Fig. 5 we illustrate the effect of initial momentum and heat fluxes on the transient behavior of both $\overline{w'^2}$ and the Reynolds stress $\overline{u'w'}$. The solid curves are for no initial momentum or heat flux. The initial fluxes for the dashed curves are based on the equilibrium solution for a Richardson number of - 0.1 i.e., for an initially unstable shear layer. Steady state is reached in about 4 hours for both cases.

Superequilibrium

If one is not concerned with the transient behavior of turbulence in the stratosphere and requires only the equilibrium turbulent flow field, then Eqs. (22) to (28) can be reduced to a set of seven simultaneous algebraic equations by using the following three assumptions:

1. All correlations are in local equilibrium and, therefore $D/Dt \equiv 0$.

2. The diffusive terms are negligible and may be omitted.

3. The Reynolds number is large and, therefore, viscous terms can be neglected.

We refer to the resulting equations as the "superequilibrium" equations and summarize them below.

$$0 = - 2 \overline{u'w'} \frac{\partial \overline{u}}{\partial z} - \frac{q}{\Lambda_1} (1 + 2b\beta) \overline{u'^2} + \frac{q^3}{3\Lambda_1} [1 - 2b(1 - \beta)] \quad (30)$$

$$0 = - \frac{q}{\Lambda_1} (1 + 2b\beta) \overline{v'^2} + \frac{q^3}{3\Lambda_1} [1 - 2b(1 - \beta)] \quad (31)$$

$$0 = \frac{2g}{\overline{T}_o} \overline{w'T'} - \frac{q}{\Lambda_1} (1 + 2b\beta) \overline{w'^2} + \frac{q^3}{3\Lambda_1} [1 - 2b(1 - \beta)] \quad (32)$$

$$0 = - \overline{w'^2} \frac{\partial \overline{u}}{\partial z} + \frac{g}{\overline{T}_o} \frac{\partial \overline{T}}{\partial z} - \frac{q}{\Lambda_1} (1 + 2b\beta) \overline{u'w'} \quad (33)$$

$$0 = - \overline{u'w'} \frac{\partial \overline{T}}{\partial z} - \overline{w'T'} \frac{\partial \overline{u}}{\partial z} - \frac{qA}{\Lambda_1} \overline{u'T'} \quad (34)$$

$$0 = - \overline{w'^2} \frac{\partial \overline{T}}{\partial z} + \frac{g}{T_o} \overline{T'^2} - \frac{qA}{\Lambda_1} \overline{w'T'} \tag{35}$$

$$0 = - 2 \overline{w'T'} \frac{\partial \overline{T}}{\partial z} - \frac{2bsq}{\Lambda_1} \overline{T'^2} \tag{36}$$

In the above equations, we have utilized assumption 3 to rewrite Eq. (29) as

$$\lambda^2 = \frac{\Lambda_1^2}{a + b \frac{q\Lambda_1}{\nu_o}} = \frac{\nu_o \Lambda_1}{bq} \tag{37}$$

If we now introduce the following definitions into Eqs. (30) to (35)

$$\overline{u'^2} = UU\Lambda_1^2 \left(\frac{\partial \overline{u}}{\partial z} \right)^2$$

$$\overline{v'^2} = VV\Lambda_1^2 \left(\frac{\partial \overline{u}}{\partial z} \right)^2$$

$$\overline{w'^2} = WW\Lambda_1^2 \left(\frac{\partial \overline{u}}{\partial z} \right)^2$$

$$\overline{u'w'} = UW\Lambda_1^2 \left(\frac{\partial \overline{u}}{\partial z} \right)^2$$

$$\overline{u'T'} = UT\Lambda_1^2 \frac{\partial \overline{u}}{\partial z} \frac{\partial \overline{T}}{\partial z}$$

$$\overline{w'T'} = WT\Lambda_1^2 \frac{\partial \overline{u}}{\partial z} \frac{\partial \overline{T}}{\partial z}$$

$$\overline{T'^2} = TT\Lambda_1^2 \left(\frac{\partial \overline{T}}{\partial z} \right)^2$$

$$q^2 = \overline{u'^2} + \overline{v'^2} + \overline{w'^2} = QQ\Lambda_1^2 \left(\frac{\partial \overline{u}}{\partial z} \right)^2 \tag{38}$$

then we can summarize the system of equations in the following compact form.

$$Q(1 + 2b\beta)UU = \frac{Q^3}{3}[1 - 2b(1 - \beta)] - 2UW \tag{39}$$

$$Q(1 + 2b\beta)VV = \frac{Q^3}{3}[1 - 2b(1 - \beta)] \tag{40}$$

$$Q(1 + 2b\beta)WW = \frac{Q^3}{3}[1 - 2b(1 - \beta)] + 2Ri \cdot WT \tag{41}$$

$$Q(1 + 2b\beta)UW = - WW + Ri \cdot UT \tag{42}$$

$$Q \cdot A \cdot UT = - UW - WT \tag{43}$$

$$Q \cdot A \cdot WT = - WW + Ri \cdot TT \tag{44}$$

$$Q \cdot b \cdot S \cdot TT = - WT \tag{45}$$

In these equations, Ri is the Richardson number

$$Ri = \frac{g}{\overline{T}_o} \frac{\partial \overline{T}}{\partial z} \Big/ \left(\frac{\partial \overline{u}}{\partial z} \right)^2 \tag{46}$$

Therefore, we have seven algebraic equations which are a function of Ri and the model parameters b, β, A and S . The solutions of the equations for values of the model parameters summarized previously are shown in Figs. 6 to 9. Results are shown for both stable (positive Ri) and unstable (negative Ri) environments. The equilibrium turbulence is zero for $Ri > 0.55$, i.e., the equilibrium flow field is laminar.

We can demonstrate the accuracy of superequilibrium theory by recomputing the effects of wind shear on the correlations. We consider a temperature gradient of 1 deg/km and a scale length of 15 m, conditions which correspond to the calculations summarized in Fig. 1 and Table 1. Superequilibrium results are shown by the solid lines in Figs. 10 and 11. These figures graphically illustrate the strong dependence of the correlations on the wind shear.

The symbols on Figs. 10 and 11 are the data from Table 1 which were obtained using the complete invariant model. The accuracy of superequilibrium is readily apparent. Therefore, if the local $Ri < Ri_{crit}$, then superequilibrium can be used to determine the turbulent flow field. When the local Ri is greater than Ri_{crit}, the crucial question is, "How fast does the turbulence decay to a laminar state?" Superequilibrium cannot help us and we must resort to the complete system of equations.

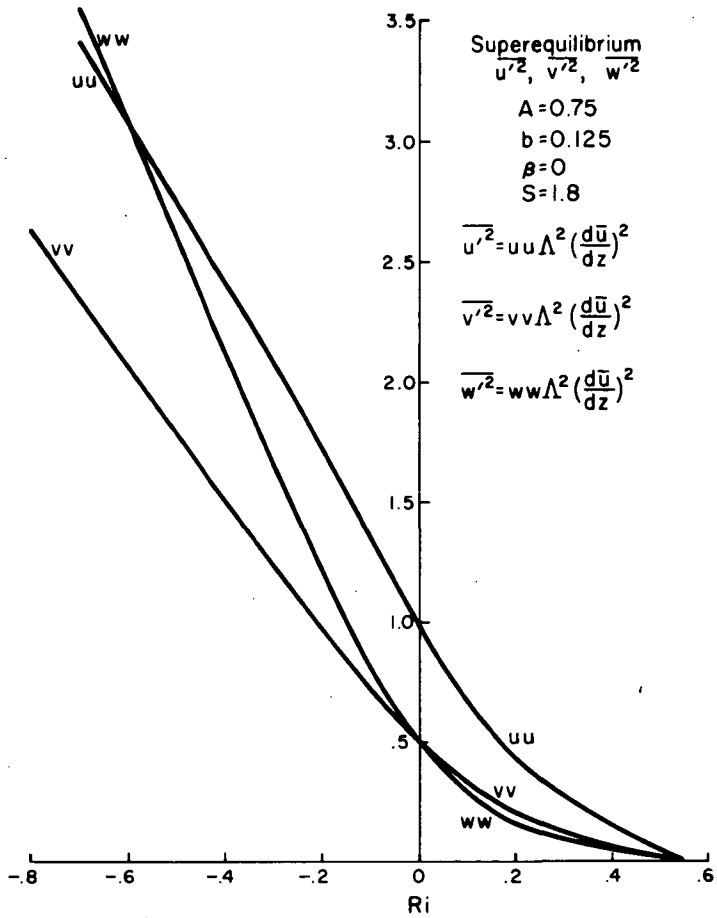

Figure 6. Superequilibrium solutions for the turbulent kinetic energies, $\overline{u'^2}$, $\overline{v'^2}$, and $\overline{w'^2}$.

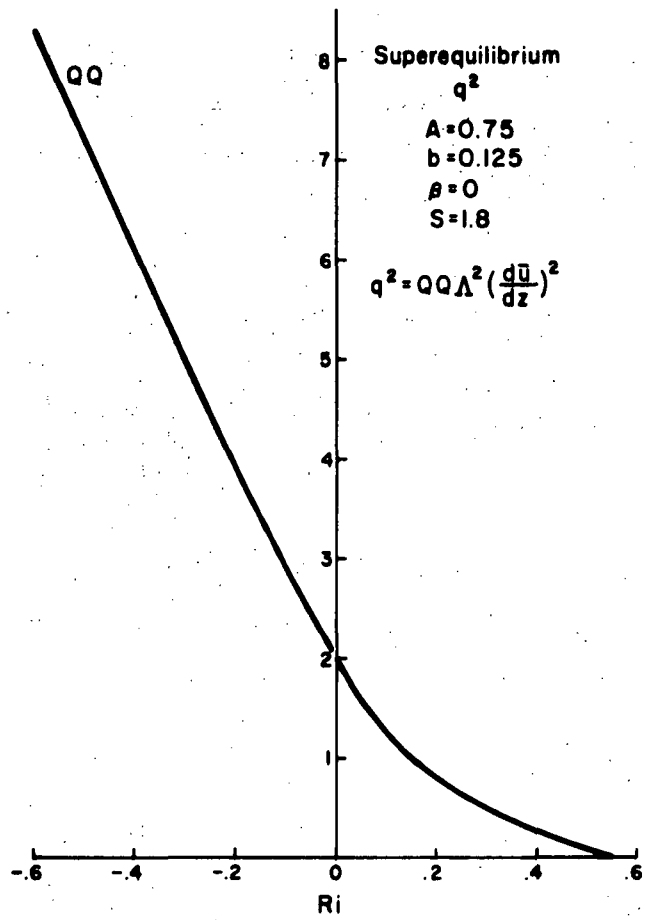

Figure 7. Superequilibrium solutions for total turbulent kinetic energy, $q^2 = \overline{u'^2} + \overline{v'^2} + \overline{w'^2}$.

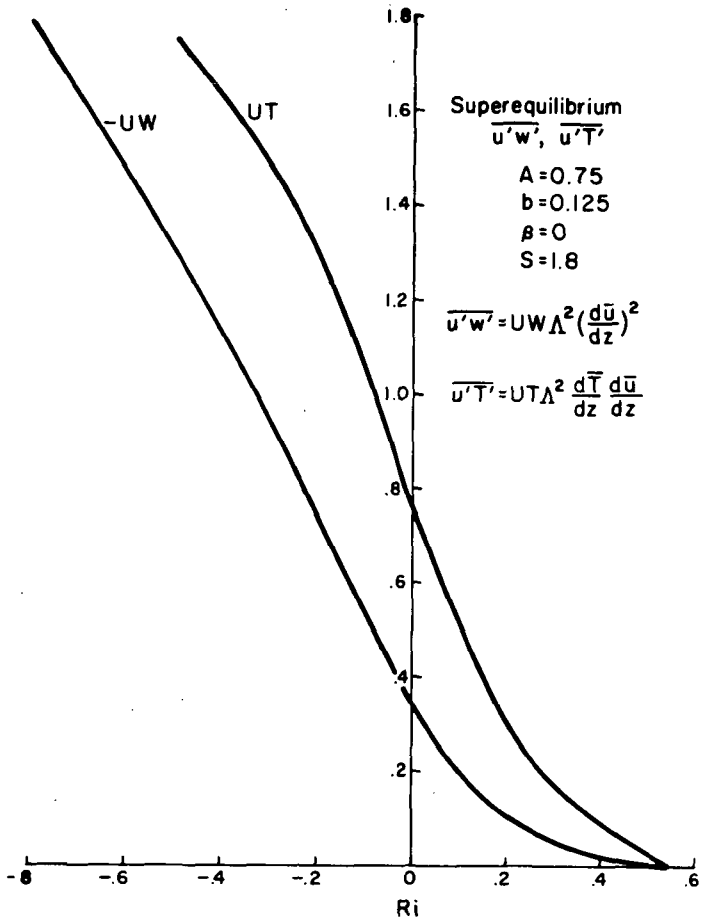

Figure 8. Superequilibrium solutions for shear stress, $\overline{u'w'}$, and longitudinal heat flux, $\overline{u'T'}$.

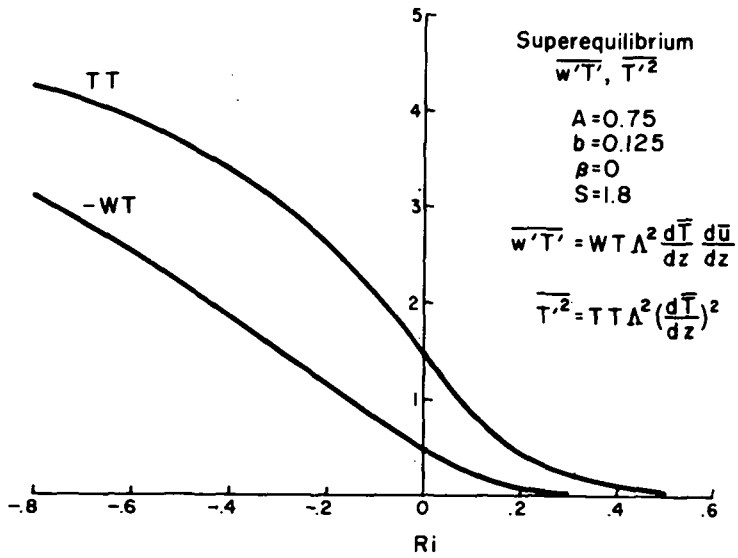

Figure 9. Superequilibrium solutions for vertical heat flux, $\overline{w'T'}$, and temperature fluctuation variance, $\overline{T'^2}$.

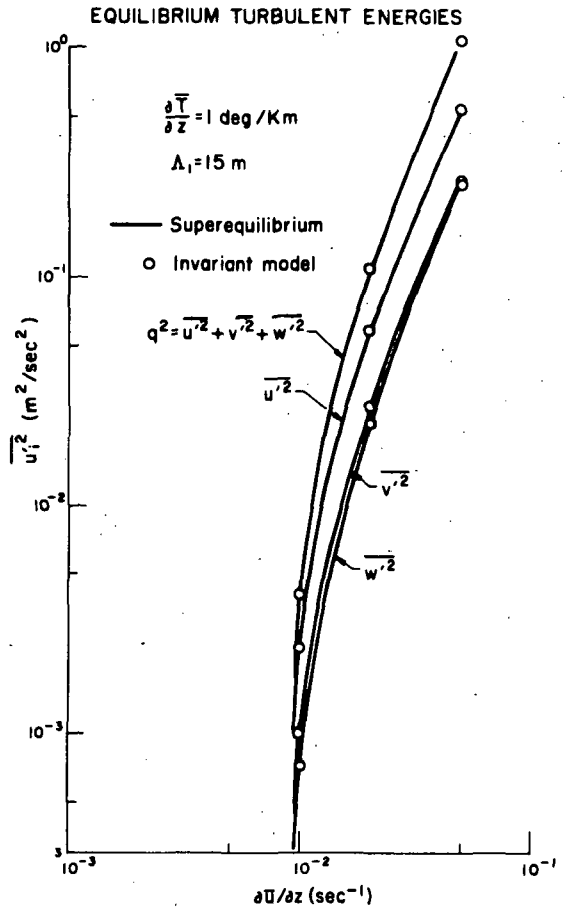

Figure 10. Equilibrium turbulent energies as calculated from full model and from superequilibrium approximations and for a range of wind shear conditions.

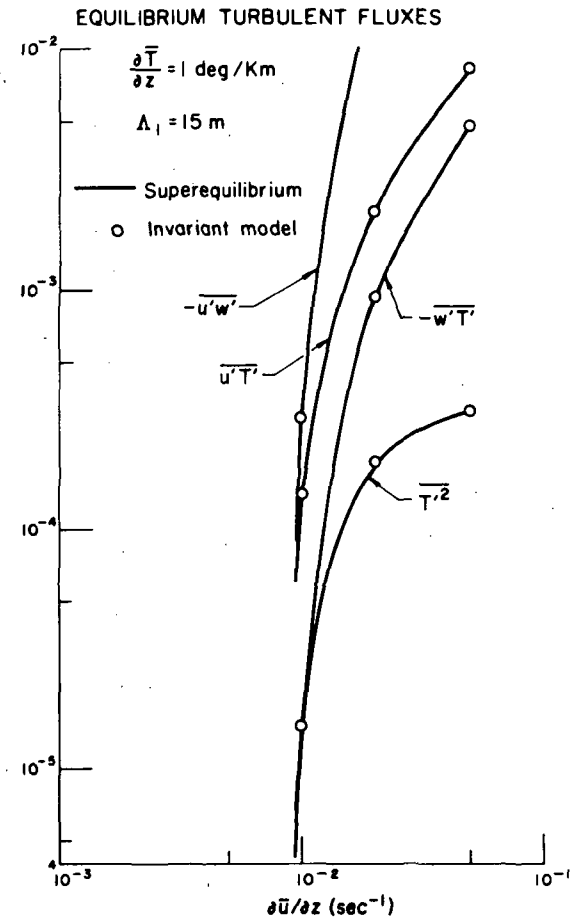

Figure 11. Equilibrium turbulent fluxes of heat and momentum for same conditions used in Figure 10.

Analyses of the Decay of Turbulence when $Ri > Ri_c$

In an effort to estimate the Richardson number in the stratosphere, we have computed the wind shear and temperature gradient in the 16 to 26 km altitude interval using wind speed and temperature measurements provided by the United States Weather Bureau. Figure 12 shows the results for one day; the data are based on Northern Hemisphere Data Tabulations - May 25, 1963. The figure contains 132 data points for approximately two dozen independent measurements in the continental United States, Alaska, and ships in the Atlantic.

The most significant point to note is that 99% of the data are for a Richardson number greater than ten, a value considerably in excess of the critical value. In addition, 90% of the points lie in the stable regime $(d\overline{T}/dz > 0)$. Admittedly, these data are for one day only. However, they do suggest that, for the most part, the atmosphere is laminar at SST cruise altitudes.

If the stratosphere is indeed laminar, then how rapidly do turbulent bursts decay? And, does the decay rate vary with wind shear, stability, scale length or initial energy level? The following analyses attempt to answer these questions.

In Fig. 13 we show the turbulent energy decay for three scale lengths. The wind shear ($.005\ sec^{-1}$) and potential temperature gradient (1 deg/km) are such that the Richardson number (1.8) is greater than the critical value.

Several points should be noted. First, the decay rate eventually reaches a constant value (the power law exponent is approximately - 1.8) which is independent of scale length. Secondly, in the constant decay rate region, the curves are displaced by a time proportional to Λ_1. Finally, and perhaps most significantly, the turbulent energy decays to less than 1% of its initial value $(q^2(t) = .009\ m^2/sec^2)$ within 15 minutes to 3 hours.

The direct scaling of the decay curve with Λ_1 suggests that proper normalization of the time might yield universal decay curves. In Fig. 14 we have redrawn the data with the independent variable being $q_o\ t/\Lambda_1$. With these variables, the decay curves virtually coalesce.

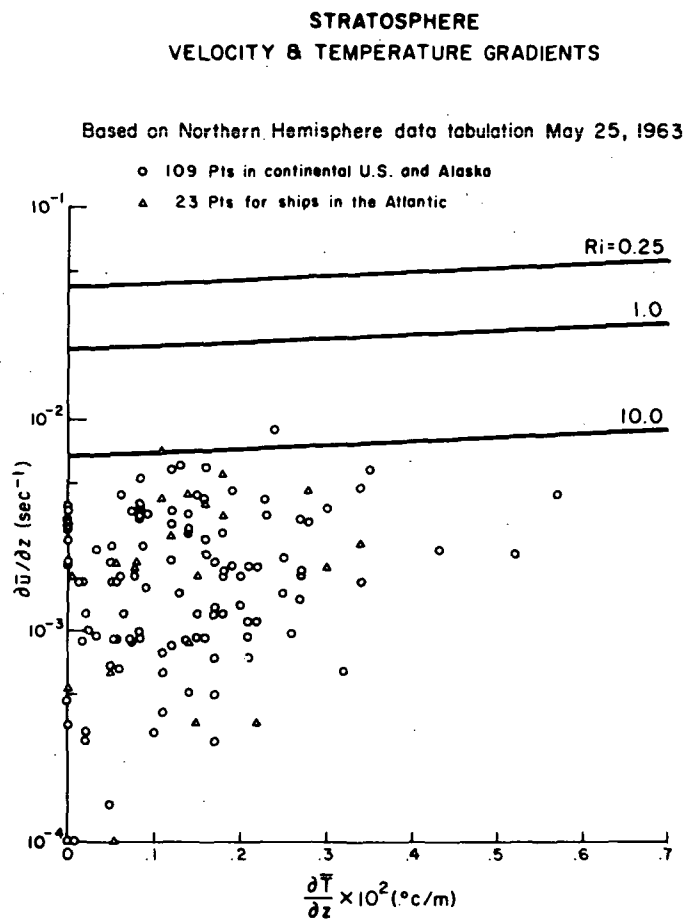

Figure 12. Calculated values of Ri as derived from one day's observations of wind and temperature between 18 and 26 km altitude over North America and the North Atlantic.

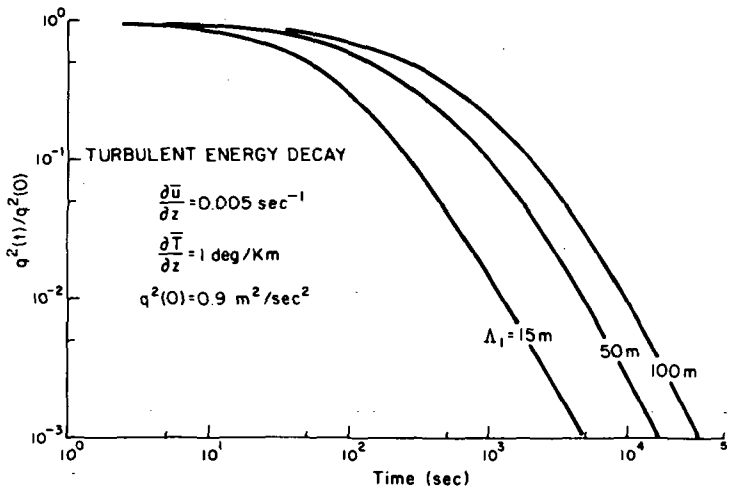

Figure 13. Calculated turbulent energy decay histories for Ri = 1.8.

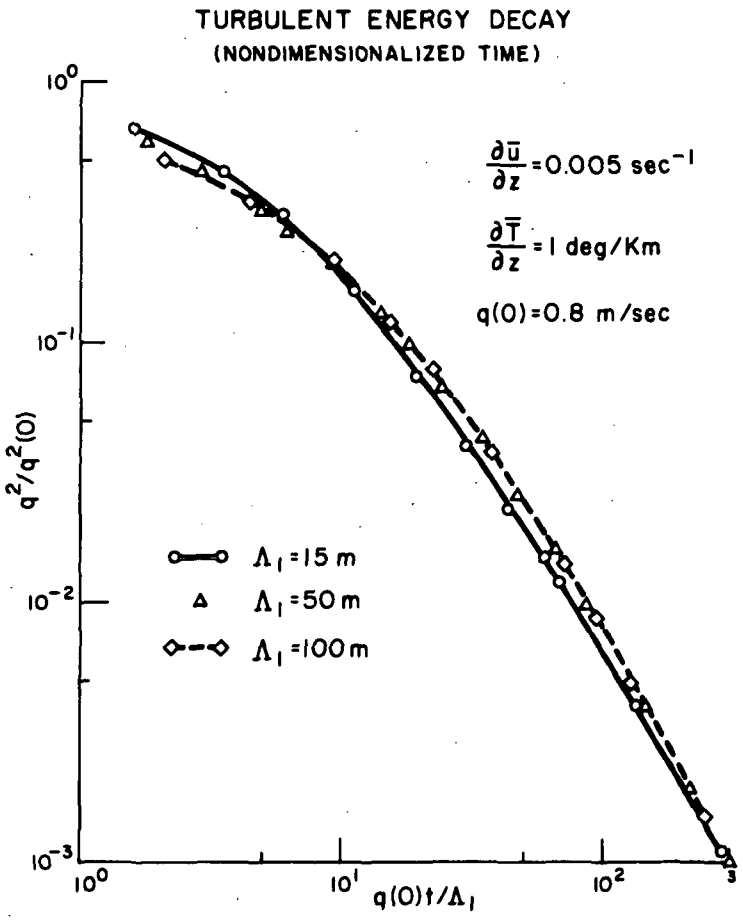

Figure 14. Turbulent decay histories normalized by $q_o t/\Lambda_1$.

How universal is this decay curve? To answer this question, we examine the effect of wind shear and stability on turbulence energy decay. Figure 15 shows that the effect of wind shear on the decay rate is insignificant. A shear decrease of one order of magnitude decreases the time required to reach 1% of the initial energy approximately 2 minutes. A similar effect can be noted in Fig. 16 for an order of magnitude change in the temperature gradient. We conclude that shear and stability have a second order influence on the turbulence energy decay rate when $Ri > Ri_{crit}$.

Having considered the effects of shear and stability, we can now examine the effect of the initial turbulence profile on the turbulent energy decay rate. In Fig. 17 we illustrate the effect of initial turbulent energy. It is evident that the normalized curves virtually coincide even for a two order-of-magnitude change in initial energy. However, because q_o appears in the normalized variables, it is not immediately obvious how the turbulence residence time varies with initial energy level. If, for purposes of discussion, we arbitrarily set a detectability limit on q^2 of .06 m^2/sec^2, then the turbulence residence time is 20 minutes for $q_o^2 = .6$ m^2/sec^2 and 30 minutes for $q_o^2 = 60$ m^2/sec^2. In other words, as the time required to reach the limit of detectability increases, then the initial kinetic energy has less influence on the residence time.

In Fig. 18 we illustrate the effect of the initial momentum and heat fluxes on the decay rate. Of course, there are an infinite number of possible initial turbulence states. We have chosen to illustrate two. We define one state as an equilibrium profile because the initial conditions are based on the equilibrium state for $Ri = 0.2$ and $q_o = 10$ m/sec . The nonequilibrium curve is based on the same initial energy distribution but the initial fluxes ($\overline{u'T'}$, $\overline{w'T'}$, $\overline{u'w'}$ and $\overline{T'^2}$) are an order-of-magnitude larger. Again, the universal nature of the decay curve is evident.

Having discussed the results of computations using the complete invariant model, we can simplify matters considerably if we assume that the turbulent energy decay rate is primarily governed by the dissipation term in the equation for q^2 (obtained by summing Eqs. (22), (23) and (24)). Then we have

$$\frac{dq^2}{dt} = - \frac{2bq^3}{\Lambda_1} \qquad (47)$$

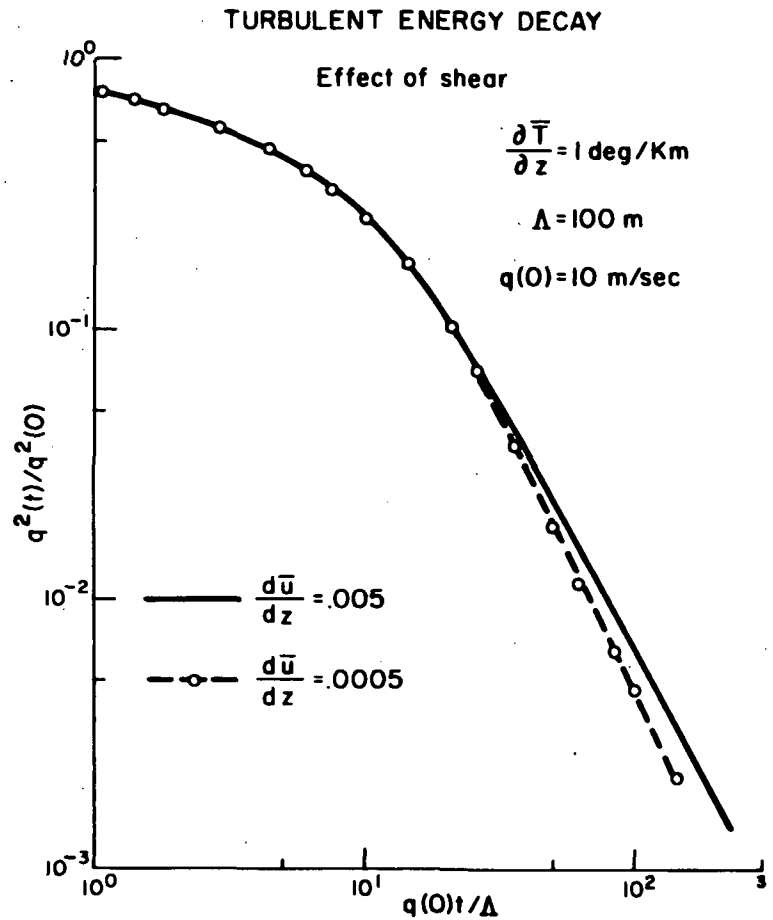

Figure 15. Calculations of turbulent energy decay for two wind shear conditions.

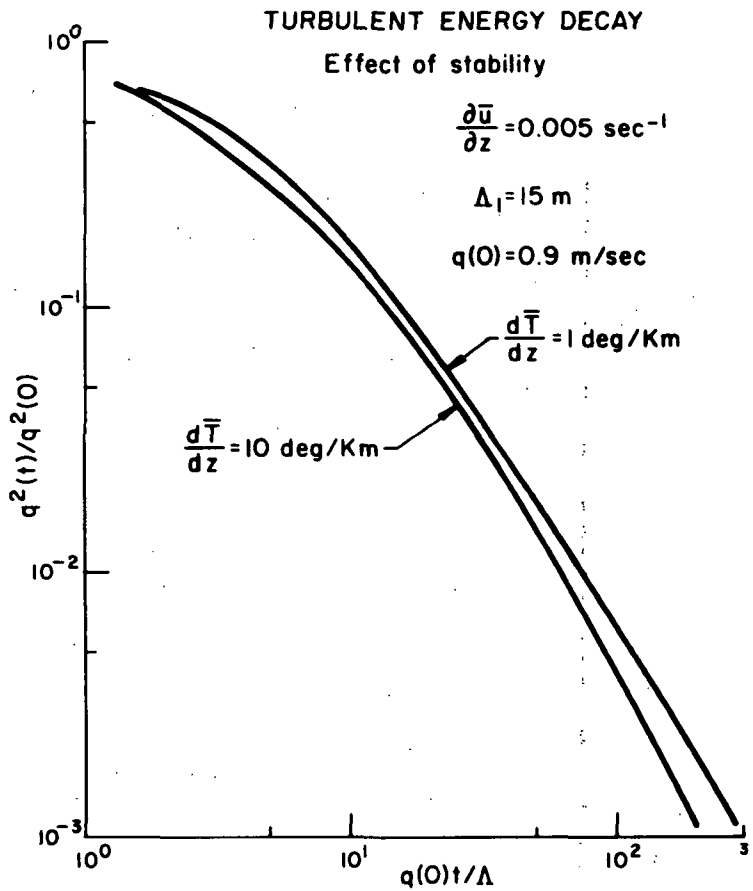

Figure 16. Calculations of turbulent energy decay for two stability classes.

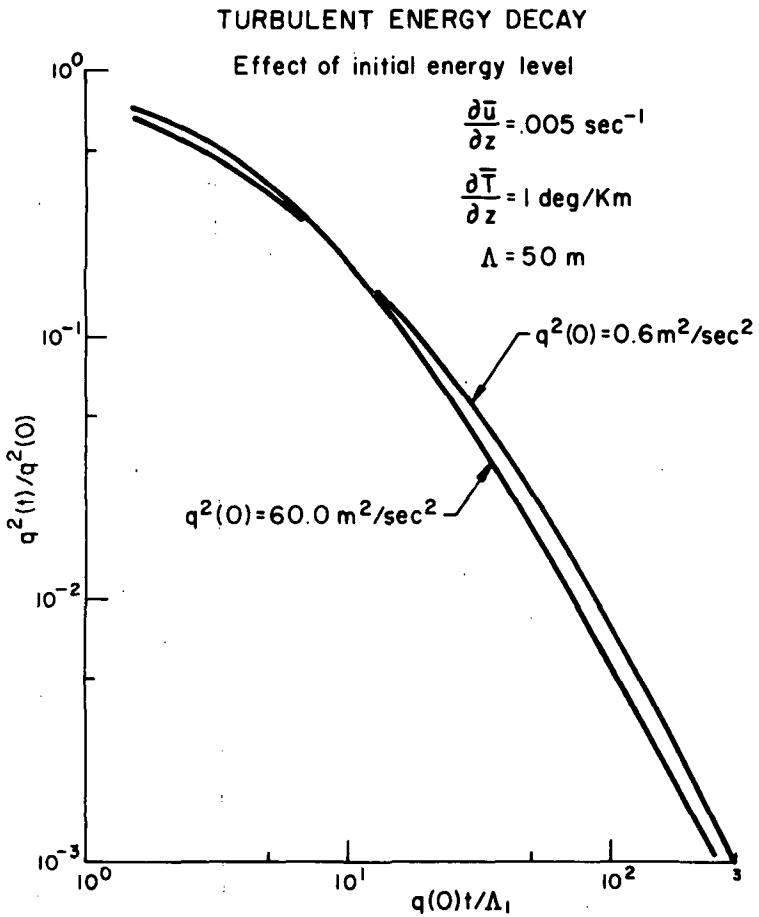

Figure 17. Effect of initial turbulent energy value on decay rates.

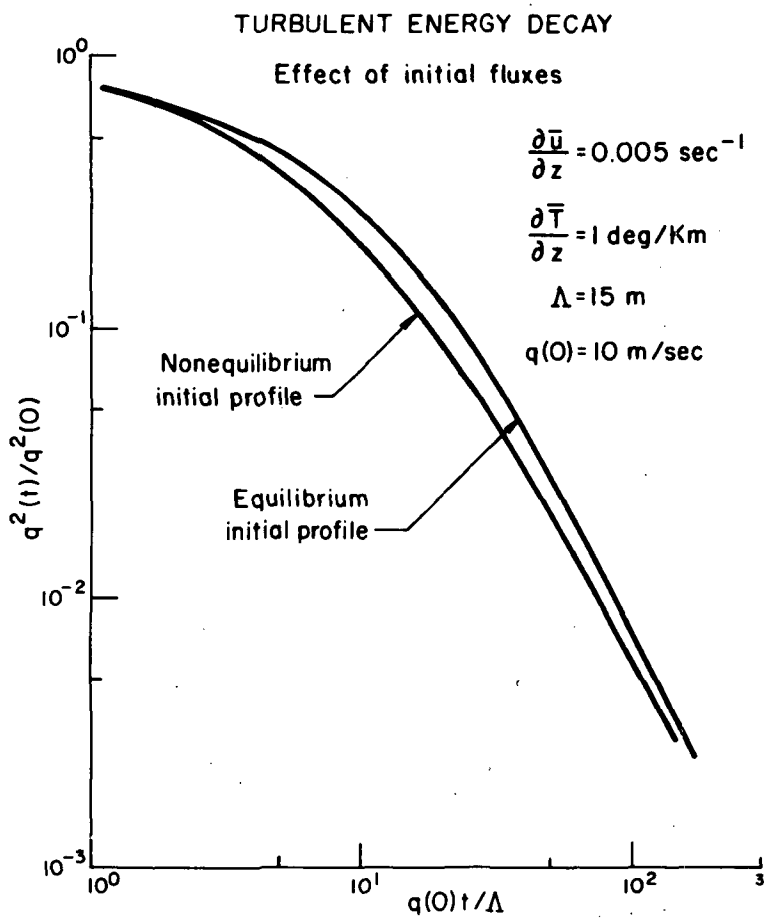

Figure 18. Effect of initial fluxes of heat and momentum on turbulence decay rates.

If Λ_1 = constant (the case we have considered thus far), then Eq. (47) can be integrated to yield

$$\frac{q}{q_o} = \frac{1}{1 + \frac{q_o bt}{\Lambda_1}} \tag{48}$$

where b has the value 0.125. In Fig. 19 the decay rate based on Eq. (48) is compared to a typical decay curve based on the complete invariant model. We note that Eq. (48) gives a satisfactory prediction of the decay rate. This is not too surprising since we postulated that the dissipation term was the dominant factor in the decay rate. However, we can get more useful information from Eq. (48). In particular, as t becomes large Eq. (48) goes to the limit

$$q(t) = \frac{\Lambda_1}{bt} \tag{49}$$

Thus, q(t) is directly proportional to Λ_1 (as we showed in Fig. 13) and does not depend on shear, stability or the initial conditions.

The Problem of Scale Length

Although Eq. (47) shows the influence of scale length on turbulent decay, it sheds little light on the appropriate scale length to use. We have therefore, begun to investigate the effect of variable scale length on the decay of turbulence. Some of our work in other areas suggests that the scale length depends on the turbulent energy and the Brunt - Väisälä frequency, N , such that

$$\Lambda_1 = \frac{q}{2N} \tag{50}$$

where $N = (g/\overline{T}\ \partial\overline{T}/\partial z)^{\frac{1}{2}}$ and $\overline{T}$ is the potential temperature. If we substitute Eq. (50) into Eq. (47) and integrate we get

$$\frac{q^2(t)}{q_o^2} = e^{-4bNt} \tag{51}$$

which is a more rapid decay rate than that given by Eq. (48). We illustrate this decay rate in Fig. 20 and observe that the turbulence energy is dissipated to $10^{-3} \times q_o^2$ within 30 minutes, compared to approximately 5 hours for the constant Λ = 50 m case. Because the constant scale length assumption yields the longest turbulence residence times, that assumption provides the more conservative estimate for the diffusion of SST exhaust products.

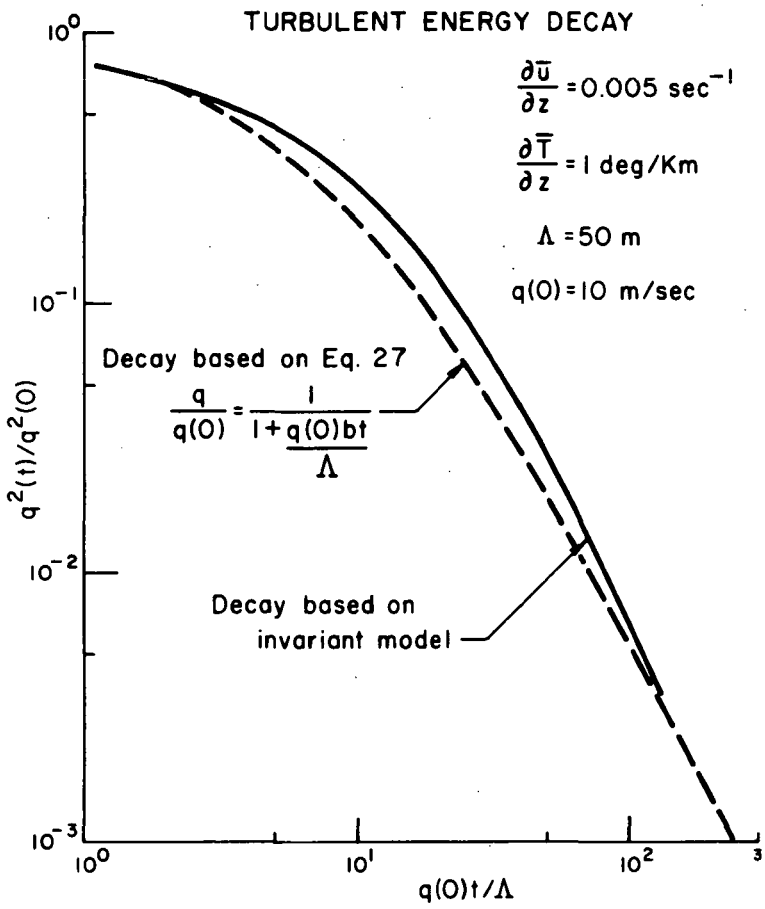

Figure 19. Comparison of turbulence decay rates calculated from full model to those calculated from the dissipation term alone.

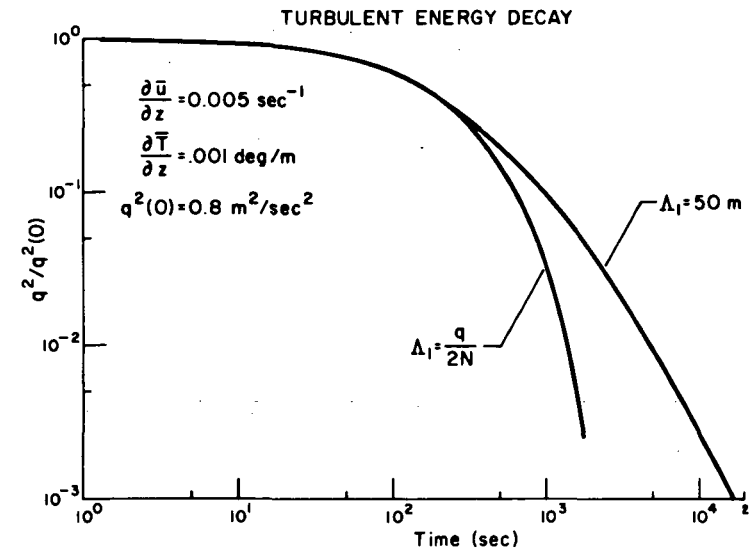

Figure 20. Comparison of turbulence decay rates for two assumptions regarding the macro-scale length, Λ_1 .

At this point, however, we must note that the lack of definitive observations of either the steady-state turbulence or the decay of externally induced turbulence is a serious handicap in choosing among turbulence simulation models. And, as the foregoing analyses show, the primary uncertainty in these estimates is resident in the lack of specificity of the scale length defined as Λ_1 in second-order closure models. From a physical point of view, this scale length should associate with the integral spatial scale length, i.e., it should depend upon the distance over which the small-scale turbulent motions are correlated. Attempts to estimate this scale length from aircraft traverses of detectable turbulence patches suggests Λ_1 of the order of hundreds of meters. Similarly observations of smoke puff growth can be used to infer effective scale lengths of the order of 50 to 100 m when the turbulence levels are apparently below the threshold of aircraft detectability.

These fragmentary observations provide some guidance for the calculations that follow, but it must be recognized that this critical parameter is not known within a factor of two or more, and therefore estimates of turbulence properties, such as the turbulent kinetic energy, are uncertain within at least a factor of four of their true values. The consequences of this uncertainty in the estimation of diffusion and chemical reaction rates are estimated in the next sections. For now, we may note again that only a much more adequate and appropriate experimental measurements program for turbulence fields in the lower stratosphere can reduce these uncertainties.

The Choices of Turbulence Fields for SST Wake Calculations

The results of invariant model simulations of turbulence fields in the lower stratosphere have been reported extensively in the last section for two reasons, 1) to examine the range of possible turbulence fields, and 2) to provide an input to other models of the turbulent diffusion of SST exhausts. If one is willing to assume a steady field of turbulence (and most modelers do make this assumption for relatively long periods of time in the diffusion process), then the superequilibrium estimates of turbulence, given wind shear, stability and an estimate of Λ_1, are particularly convenient, since all of the turbulence characteristics (through second-order moments) are readily determined.

For a first-order estimate of the significance of the turbulence field to the time-rate of dilution of Phase III SST exhaust wakes we have chosen to calculate the three-dimensional time history of the diffusion of the plume for five fields of turbulence ranging from q^2 (the turbulent kinetic energy) equal to .006 to 0.5 m^2/sec^2. These analyses are discussed in the next section.

For estimates of the joint effects of diffusion and chemistry, we have emphasized an expected value of q^2 of 0.08 m^2/sec^2 to illustrate the interactions of these processes and have then extended the calculations to the previous range of q^2 to examine the chemical efficiency of NO destruction of O_3 during the Phase III wake period. These results are discussed in the second following section. Both of these analyses assume a steady and continuous field of turbulence.

Since there is a real possibility that turbulence and diffusion in the lower stratosphere is not steady, we have constructed a preliminary model of diffusion involving aperiodic turbulence "bursts" which decay to laminar flow and have analyzed the diffusive growth and chemical efficiency of plumes subjected to this kind of turbulence. The turbulence fields chosen for this example are discussed in context in the third following section.

ESTIMATES OF THE DIFFUSION OF NONREACTIVE EXHAUST PRODUCTS

In the analyses of the Phase III wake period for SST exhaust materials, a natural first question in the context of CIAP evaluations is, "How long does this Phase last?" For one thing, this is the period of time during which the behavior (transport and diffusion) of the plumes is within the spatial- and time-scale resolutions of the large-scale global transport models. For another, during this period individual plumes represent localized anomalies of exhaust material concentrations and exhibit the greatest departures from the mean values used in large-scale chemical kinetics calculations. The significance of such departures is, of course, heavily weighted by how long they persist.

A second general question of interest to CIAP is the relative extent to which the plumes are diffused laterally and vertically (the anisotropic nature of the diffusion), during the Phase III wake period. These estimates serve directly in describing the concentration distributions when the plumes achieve the grid-scale dimensions of the global transport models and they can be used to estimate the effective eddy diffusivities for first-order closure plume models.

In order to estimate these basic parameters of Phase III diffusion processes for a variety of steady turbulence fields, we have calculated the three-dimensional diffusion history of a plume segment for which the initial horizontal and vertical variances of concentration were 625 m^2 (a plume width and depth of about 100 m) over the time required to dilute the plume by factors of 10^3. These calculations have been made for five turbulence fields for which the intensity of turbulence, q^2, ranged from 0.006 to

0.5 m^2/sec^2 and Ri from 0 to 0.5. (Recall $Ri_c = 0.55$ for turbulence model parameters used.)

The Duration of Phase III as a Function of Turbulence Intensity

More specifically, the five turbulence fields chosen to investigate the rates of diffusive growth and dilution of an SST plume segment are listed in Table 4. Besides these inputs, the diffusion model requires a specification of the diffusive scale length. This latter scale length is analogous to the turbulence scale length, but is not necessarily the same, since it depends upon the dimensions of the plume. (Cf. ref. 5 for a discussion of this subject.) Prior applications of this model have shown that the diffusive scale length for individual plumes is very well specified by the standard deviation of the concentration distribution until this length reaches a multiple of the turbulent scale length. For our present purposes we have chosen this multiple as five.

TABLE 4

Turbulence Characteristics Chosen For Nonreactive Diffusion Calculations

Case	q^2 (m^2/sec^2)	$\overline{v'^2}$ (m^2/sec^2)	$\overline{w'^2}$ (m^2/sec^2)	$\overline{w'T'}$ (m^oc/sec)	Remarks Ri
1	.500	.125	.125	.000	Neutral; Ri = 0
2	.210	.052	.052	-4×10^{-4}	Stable; Ri = .10
3	.100	.025	.025	-3×10^{-4}	Stable; Ri = .20
4	.034	.008	.008	-8×10^{-5}	Stable; Ri = .35
5	.006	.0014	.0014	-6×10^{-6}	Stable; Ri = .50

In order to illustrate the basic outputs of these diffusion calculations we have plotted the lateral and vertical variances of the calculated distributions, σ_y^2 and σ_z^2, and the ratio of the centerline concentration to its initial value, all as a function of time of travel. These values are shown in Figs. 21 to 25 for the cases described in Table 4.

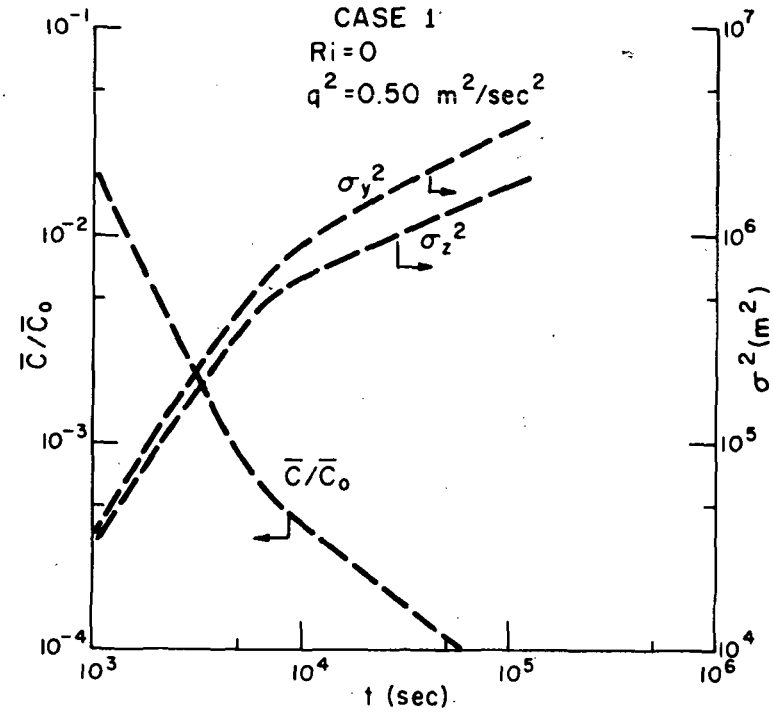

Figure 21. Calculation diffusion and plume growth for Ri = 0 and $q^2 = 0.5\ m^2/sec^2$.

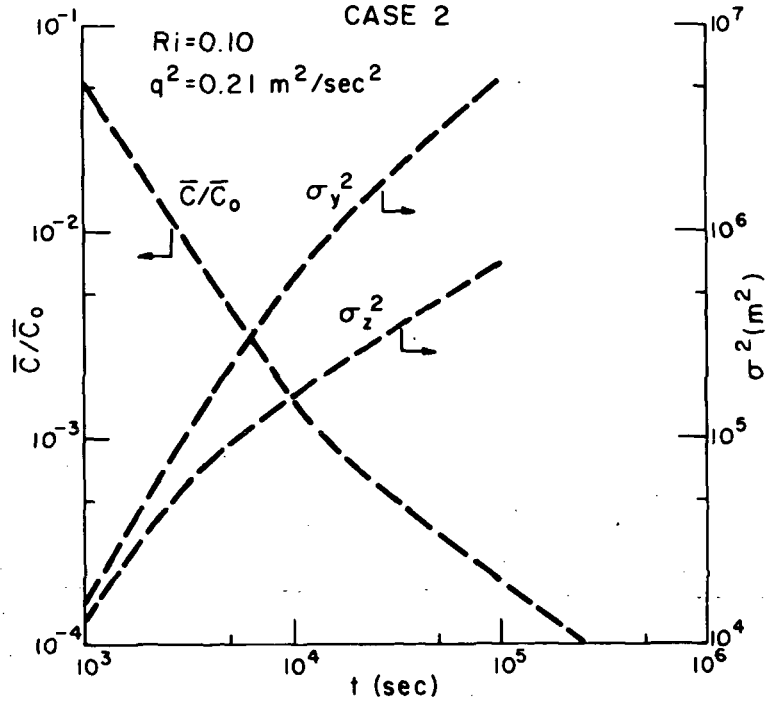

Figure 22. Same as Figure 21 but Ri = 0.10 and $q^2 = 0.21\ m^2/sec^2$.

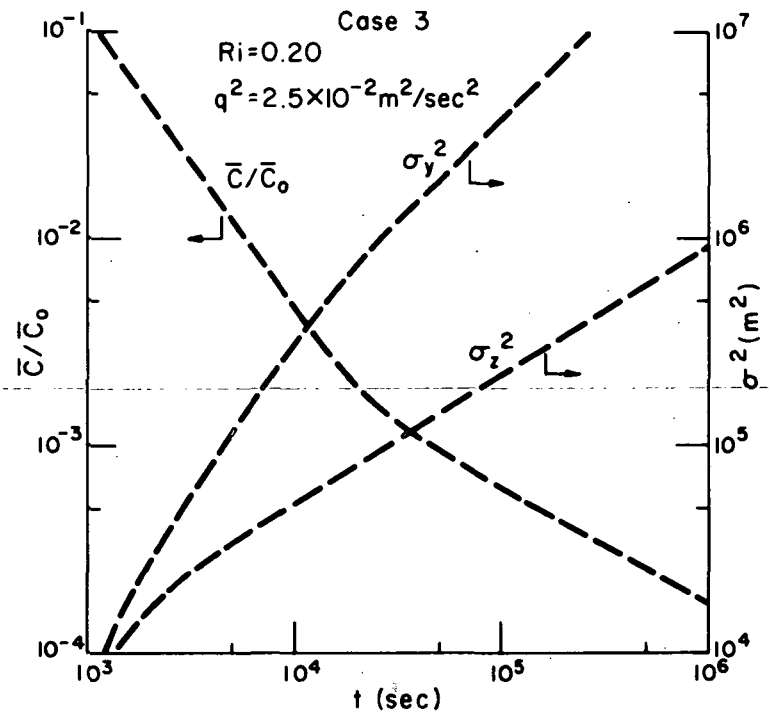

Figure 23. Same as Figure 21 but Ri = 0.20 and $q^2 = 2.5 \times 10^{-2} m^2/sec^2$.

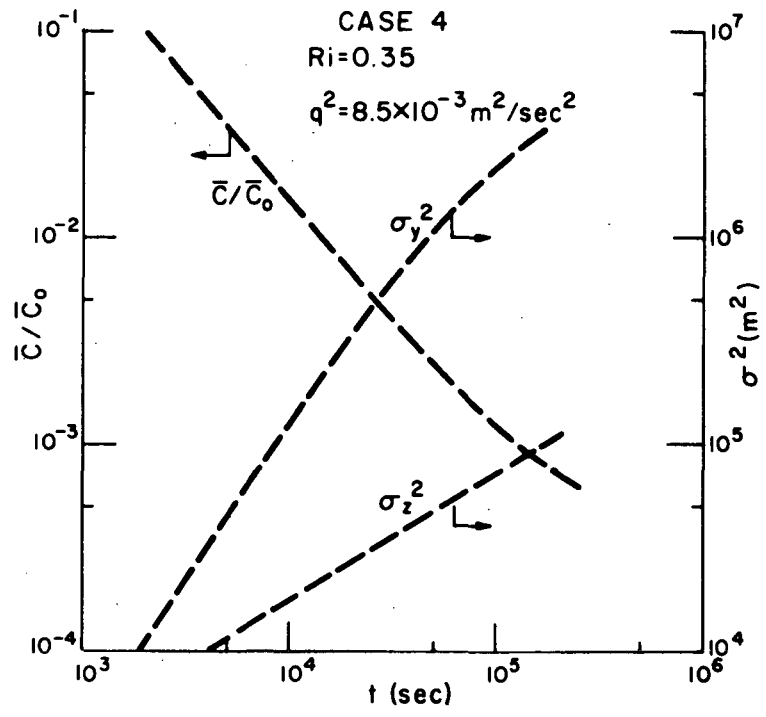

Figure 24. Same as Figure 21 but Ri = 0.35 and $q^2 = 8.5 \times 10^{-3} m^2/sec^2$.

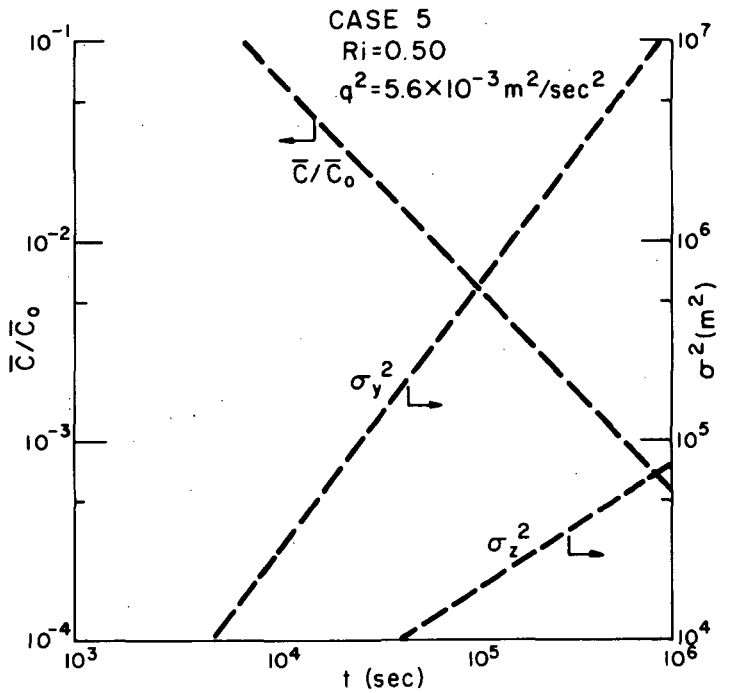

Figure 25. Same as Figure 21 but $Ri = 0.50$ and $q^2 = 5.6 \times 10^{-3}\ m^2/sec^2$.

We shall summarize pertinent information from Figs. 21 to 25 in a moment, but a visual inspection and comparison quickly shows the diffusive behavior of the plume as predicted by invariant modeling. In each case the dilution of the plume proceeds more rapidly than t^{-1} until either σ_y^2 or σ_z^2, or both, reach $2.5 \times 10^5\ m^2$, i.e., the square of the upper limit imposed on the turbulent diffusion scale length. When this limit is reached the dilution rate goes over to a lesser value, generally less than t^{-1}. Only when the turbulence is very light ($Ri \simeq Ri_c$) is the dilution rate more or less constant with time, a result expected from Fickian diffusion theory.

We can now examine the dependence of the time required to dilute the plume on the chosen field of turbulence. For this analysis we have determined the time required to reach a dilution of 10^3, t_D, and plotted this time versus the turbulent kinetic energy, q^2. These values are listed in Table 5 and plotted in Figure 26. It is very clear that the duration of Phase III is strongly dependent upon the turbulence field. For q^2 values of the order of 10^{-1} m^2/sec^2 the duration of Phase III is around 12 hours, but, if the value of q^2 is as small as 3×10^{-3} m^2/sec^2, the duration of Phase III is about 300 hours*. Similarly, an increase of one order of magnitude in the initial concentration results in an order of magnitude increase in the time required to dilute the plume to background levels, as can be seen by extrapolating the dilution curves in Figs. 21 to 25.

TABLE 5

Values of the Time, t_D, Required to Dilute a Plume Segment by a Factor of 10^3 and the Variances of the Concentration Distribution Across the Plume at that Time as Estimated for Five Fields of Turbulence

Case	q^2 $\left(\frac{m^2}{sec^2}\right)$	$\overline{v'^2}$ $\left(\frac{m^2}{sec^2}\right)$	$\overline{w'^2}$ $\left(\frac{m^2}{sec^2}\right)$	$D = 10^3$ t_D (sec)	10^3 σ_z^2 (m^2)	10^3 σ_y^2 (m^2)
1	.500	.125	.125	5×10^3	3.3×10^5	3.9×10^5
2	.210	.052	.052	1.5×10^4	2.1×10^5	9.0×10^5
3	.100	.025	.025	4×10^4	1.2×10^5	1.6×10^6
4	.034	.008	.008	1.2×10^5	8.4×10^4	2.9×10^6
5	.006	.0014	.0014	5×10^5	6.9×10^4	7.9×10^6

*This statement assumes Phase III is terminated when $D = 10^3$ and should not be taken literally.

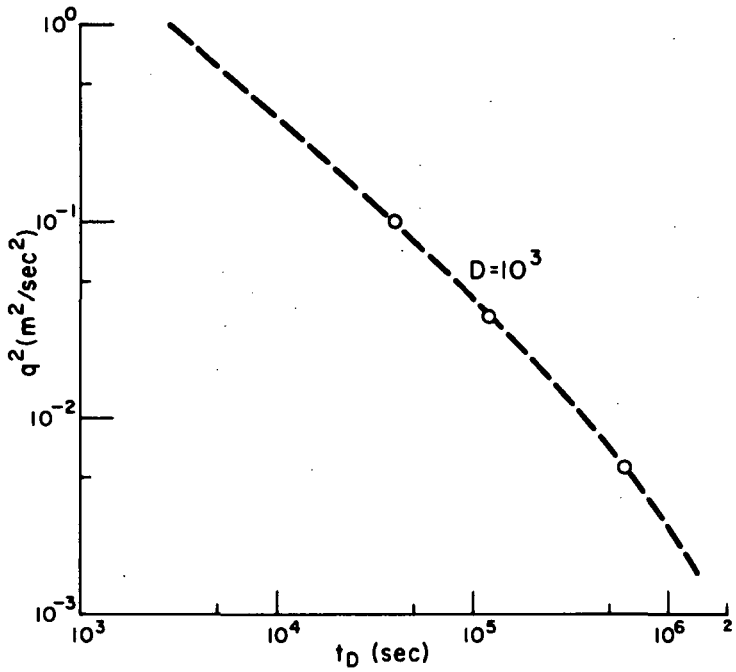

Figure 26. Calculated time required for a plume dilution of 10^3.

Since, for the most part, the lower stratosphere is stably stratified, we expect to find the lateral and vertical diffusion are not equal, and that lateral growth of the plume is significantly greater than the vertical growth. In conventional first-order closure models this anisotropy is included by selection of dissimilar effective eddy diffusivities. In second-order closure models this effect is an explicit result of the complex balance of bouyancy and mechanical forces, and does not require any arbitrary assumptions, other than for the scale lengths discussed previously.

To show the degree of anisotropy in the diffusion process for the present choices of turbulence fields, we have read out the values of σ_z^2 and σ_y^2 at the time the plume dilution reached 10^3.

These values of σ_y^2 and σ_z^2/σ_y^2 as a function of q^2 are shown in Fig. 27. (Recall from Fig. 26 that the time required to reach these values is also a strong function of q^2.) The degree of anisotropy clearly increases markedly with a decrease in the intensity of turbulence and with increases in Ri. For q^2 of the order of 10^{-2} m^2/sec^2 or less the diffusion of the plume is almost entirely in the lateral dimension.

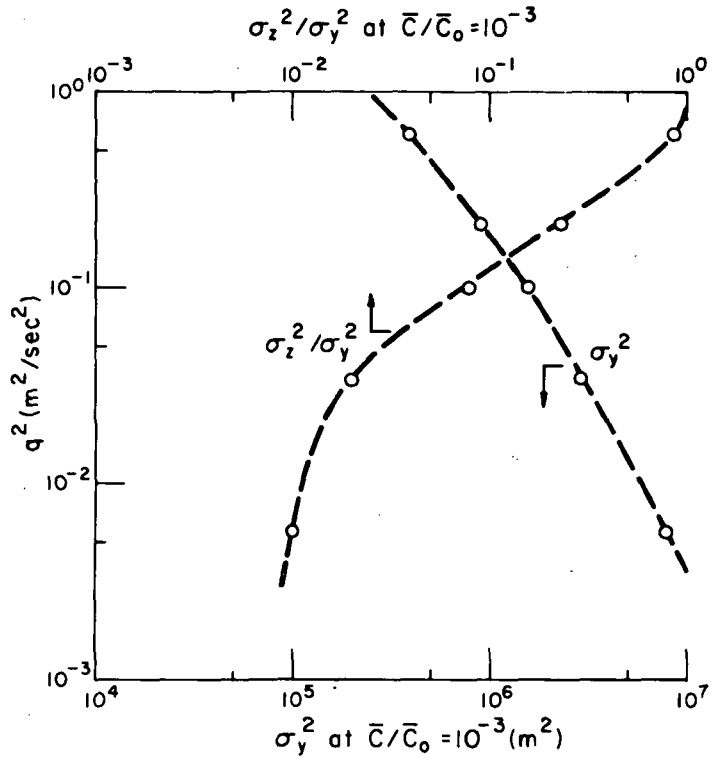

Figure 27. Calculated variances of the vertical and horizontal distributions of NO in the SST plume when they have been diluted by a factor of 10^3.

Diffusion Parameters for Conventional First-Order Closure Models

We may now relate these results of second-order closure model calculations to the parameters which would produce the same results in first-order closure models. In standard usage of these latter models we have the relationships

$$\sigma_z^2 = 2\,\overline{w'^2}\,A_z t = 2\,k_z t \tag{52}$$

and

$$\sigma_y^2 = 2\,\overline{v'^2}\,A_y t = 2\,k_y t \tag{53}$$

where, from statistical theory,

$$A_i = \int_o^\infty R_i(\xi)d\xi \tag{54}$$

and k_z and k_y are conventional eddy diffusivities. (Equations (52) and (53) are limited to times, t, for which A has become constant, i.e., $R(\xi) = 0$.) From these equations we can readily evaluate either the k's or the A's and their ratios. For example, for case three (Table 5).

$$t = 4 \times 10^4 \text{sec}$$

$$\sigma_y^2 = 1.6 \times 10^6 \text{m}^2$$

$$\sigma_z^2 = 1.2 \times 10^5 \text{m}^2$$

$$\overline{w'^2} = \overline{v'^2} = 2.5 \times 10^{-2} \text{m}^2/\text{sec}^2$$

Then

$$k_z = 1.2 \times 10^5/2 \times 4 \times 10^4 = 1.5 \text{ m}^2/\text{sec}$$

$$k_y = 1.6 \times 10^6/2 \times 4 \times 10^4 = 20 \text{ m}^2/\text{sec}$$

$$A_z = 1.2 \times 10^5/2 \times 2.5 \times 10^{-2} \times 4 \times 10^4 = 60 \text{ sec}$$

$$A_y = 1.6 \times 10^6/2 \times 2.5 \times 10^{-2} \times 4 \times 10^4 = 800 \text{ sec}$$

and

$$\frac{k_z}{k_y} = \frac{A_z}{A_y} \simeq 0.08$$

These values of k_z and k_y, of course, represent the effective diffusivities that would produce the shape and dilution of the plume calculated by the invariant diffusion model at the time the plume dilution reached 10^3. The similar values of these first-order closure model diffusion coefficients are summarized for the five cases listed in Table 6, and k_z and k_y are plotted versus q^2 in Fig. 28.

TABLE 6

Estimated Values of Diffusivity and Lagrangian Scale Length Implied by Invariant Diffusion Models

Case	q^2	$\overline{v'^2}$	$\overline{w'^2}$	t_D	k_z	k_y	A_z	A_y
	$\frac{m^2}{sec^2}$	$\frac{m^2}{sec^2}$	$\frac{m^2}{sec^2}$	(sec)	$\frac{m^2}{sec}$	$\frac{m^2}{sec}$	(sec)	(sec)
1	.500	.125	.125	5×10^3	33	39	264	312
2	.210	.052	.052	1.5×10^4	7	30	147	600
3	.100	.025	.025	4×10^4	1.5	20	60	800
4	.034	.008	.008	1.2×10^5	0.35	12	45	1500
5	.006	.0014	.0014	5×10^5	0.069	8	50	5640

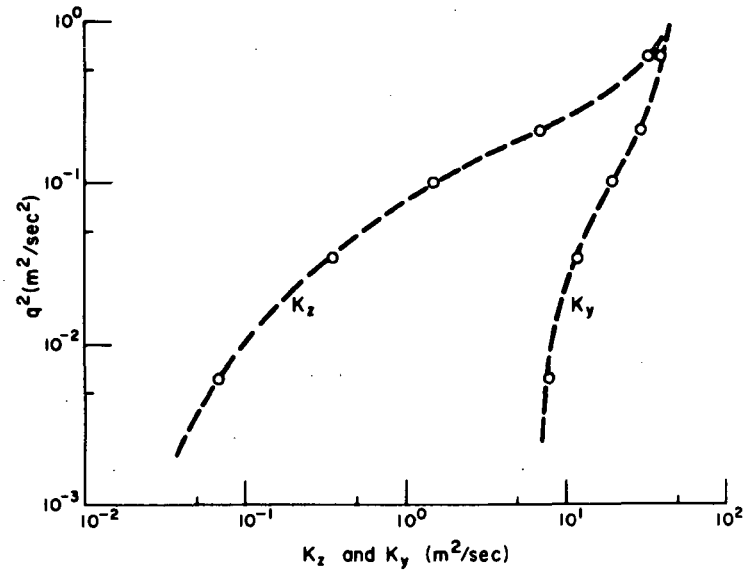

Figure 28. Values of effective eddy diffusivities, k_z and k_y, which would produce calculated concentration distributions when the SST plume has been diluted by a factor of 10^3.

In combination with the predictions of turbulent structure from known wind and temperature profiles, these estimates of effective diffusivities provide useful inputs to models using these parameters for prediction of SST plume growth. The values calculated agree reasonably well with estimates compiled by Bauer (ref. 12) if the reader bears in mind that all large scale horizontal meandering of the plume has been removed. Bauer's summary suggests a value of k_z of 1 m^2/sec, a value appropriate to a value of q^2 of about 0.1 m^2/sec^2 in the present calculation. Similarly, a comparison of k_y suggests that the expected value of 10^4 m^2/sec for the combination of diffusive growth plus meandering is made up mostly by meandering, since the diffusive component is only of the order of 10!

The primary uncertainty of these calculations resides in the choice of scale lengths. An exhaustive study of the sensitivity of the results to these choices is yet to be done, but at the present juncture it appears different choices could alter the estimates of diffusivity by about a factor of two to four.

Diffusion in Nonsteady Turbulence

The above analysis was based on the assumption of continuous diffusion in the stratosphere, a situation which is difficult to defend in the light of flight experience and the generally extreme hydrostatic stability of this region of the atmosphere ($Ri >> Ri_c$). As an alternative, we have examined the consequences of a model which assumes that for the most part the lower stratosphere is in essentially laminar flow (no significant turbulence on the scale of the SST plume dimensions), but that occasionally each volume of this part of the stratosphere experiences an externally induced burst of turbulence on this scale. This model implies that the dilution of the SST plume will be discontinuous according to a time history such as the one shown schematically in Fig. 29.

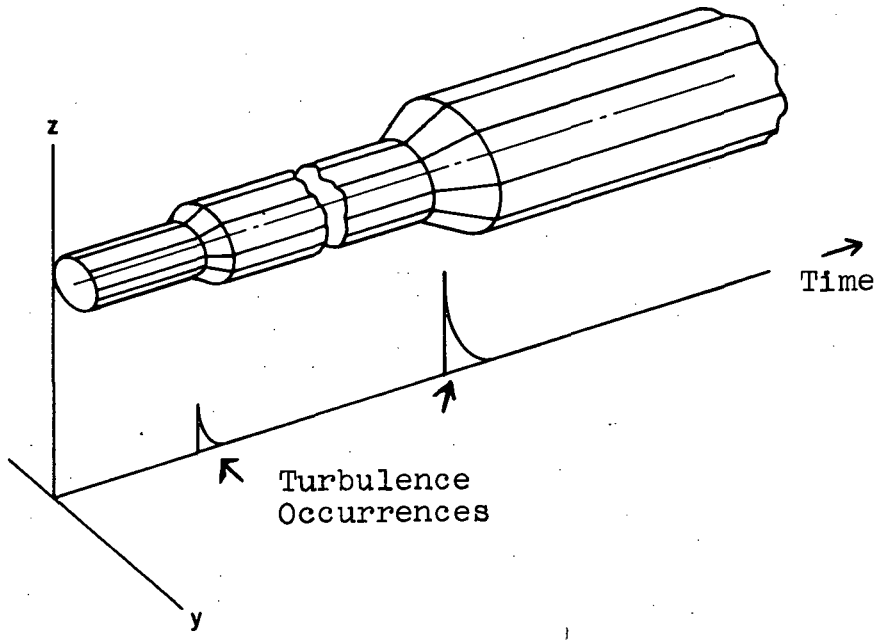

Figure 29. Schematic representation of SST plume diffusion by periodic bursts of turbulence.

A major test of this model could be obtained by observing the frequency and intensity of turbulence encountered by a free-floating balloon in the appropriate height zones of the stratosphere. Lacking these measurements, we may make some inferences regarding the recurrence period of turbulent bursts and their characteristic intensity from HI CAT data. Ashburn et al., (ref.9) has tabulated the frequency of occurrence of various levels of effective vertical gust velocities for 37 turbulence encounters above 60,000 feet. If these are converted into relative frequencies of each turbulence level one gets the plot shown in Fig. 30. Although there is some uncertainty in converting effective vertical gust velocities into turbulence intensity in three dimensions, the data do tend to show an exponential dependence of relative frequency on turbulence intensity.

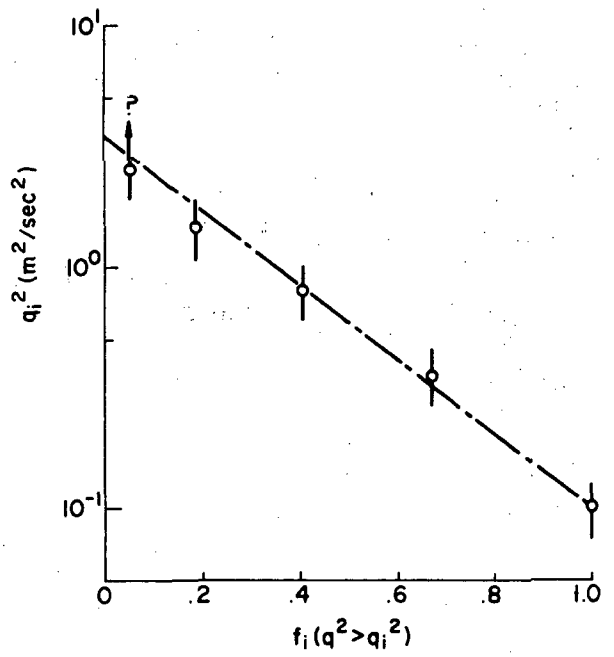

Figure 30. The relative frequency with which the intensity of turbulence, q^2, was observed to exceed the indicated value in 37 turbulence episodes sampled by HI CAT aircraft above 60,000 ft. Error bars indicate approximate uncertainty in converting vertical rms gust velocity into total turbulent kinetic energy.

Let us now assume that all of the 37 turbulence events sampled by HI CAT have a common initial intensity, that this turbulence decays at a prescribed (exponential) rate, and the HI CAT data simply reflect the probability of occurrence (the time duration) of each turbulence intensity band. Then the characteristic initial turbulence level is about 5 m^2/sec^2 and decays exponentially with time.

Using this information, we may readily deduce that the average dissipation of turbulent kinetic energy between bursts of turbulence is

$$\bar{\epsilon} = \frac{q_o^2}{2T} \tag{55}$$

where T is now the time interval between turbulence encounters for any given volume of the stratosphere and T is assumed to be large as compared with the decay time of any individual turbulence burst. Estimates of $\bar{\epsilon}$ (cf. Lilly, ref. 13) are of the order of 10^{-5} m^2/sec^3. Then

$$T = 2.5 \times 10^5 \text{ to } 2.5 \times 10^6 \text{ sec}$$

the recurrence period of turbulent bursts is between 70 and 700 hours.

We must now determine how many turbulence encounters are required to dilute a plume segment to background concentrations. As a first estimate of this quantity, we have taken advantage of the time-dependent nature of the invariant turbulence and diffusion models to estimate the decay rate of an initial turbulence burst and then the three-dimensional diffusion of a trace material embedded in this decaying turbulence field. For the turbulence calculation we have used the slower decay rate associated with a constant value of the turbulence scale length, Λ_1, as discussed in the previous section. Using an initial value of q^2 of 5 m^2/sec^2 and a value of Λ_1 of 100 m, the calculated time history of q^2 shown in Fig. 31 is obtained. Also shown there is the approximate stepped values of q^2 used in the diffusion calculation.

The results of the diffusion calculation are shown in Fig. 32 as the time histories of the lateral and vertical variances of the plume concentration distribution, σ_y^2 and σ_z^2. During the 6000 seconds of the calculation (during which the value of q^2 has decreased to 10^{-2} m^2/sec^2), σ_y^2 grows by a factor of 10^3 and σ_z^2 by a factor of 150. Since the concentration in the plume is inversely proportional to $\sigma_y \sigma_z$, the dilution during this time is about 4×10^2. Since (as will be discussed later) dilutions of the order of 10^3 to 10^4 are required, we can estimate that two or more turbulence bursts must be encountered before the Phase III plume period is terminated. Using the above estimates of the

recurrence period for turbulent bursts in the lower stratosphere, we again estimate that the duration of the Phase III period is the order of hundreds of hours, and may be as much as one or two thousand hours.

Although this model does not give drastically different estimates of the duration of Phase III, it does portray a different time history of concentrations in the plume. Assuming that diffusive mixing is negligible between turbulence encounters, a typical history of centerline concentrations for this model is shown schematically in Fig. 33. These results are elaborated as to their effect on the chemistry of the plume materials in the next section. Here we need only note that the average concentrations in the plume inferred by this model are higher than those inferred from continuous diffusion, even though the time required to dilute the plume to background concentrations is not demonstrably different.

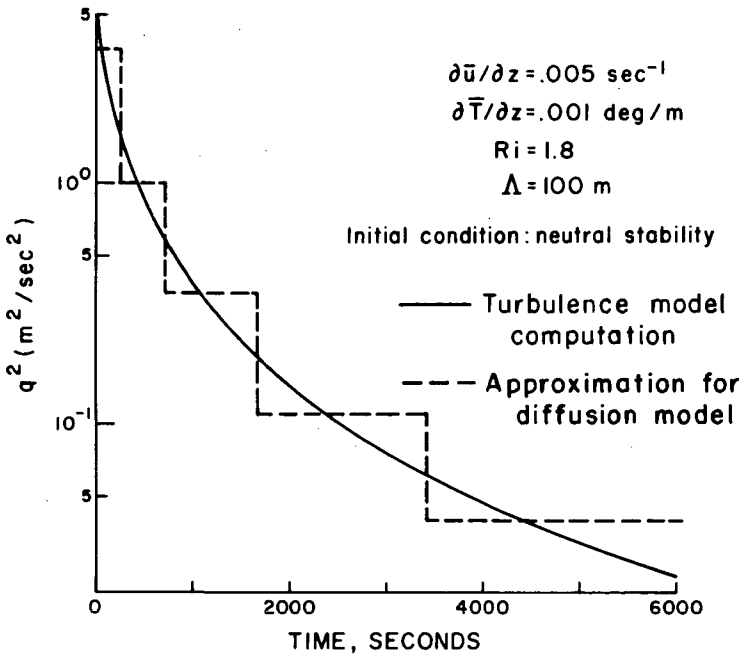

Figure 31. Turbulence decay history used for calculations of diffusion in a dying turbulence field.

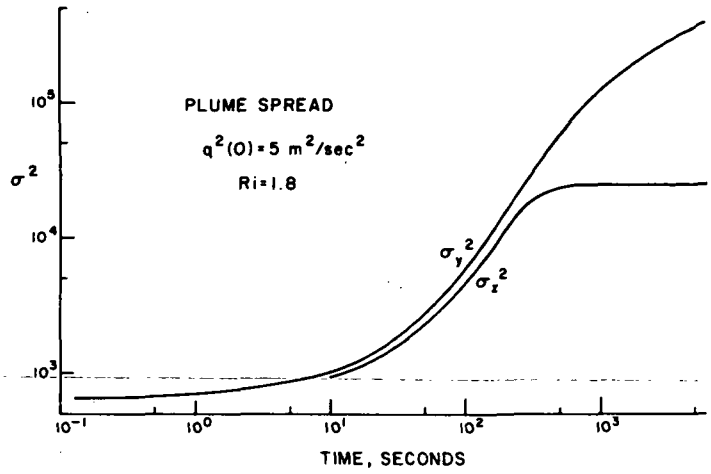

Figure 32. Time history of lateral and vertical distributions of concentration in SST plume for decaying turbulence field shown in Figure 31.

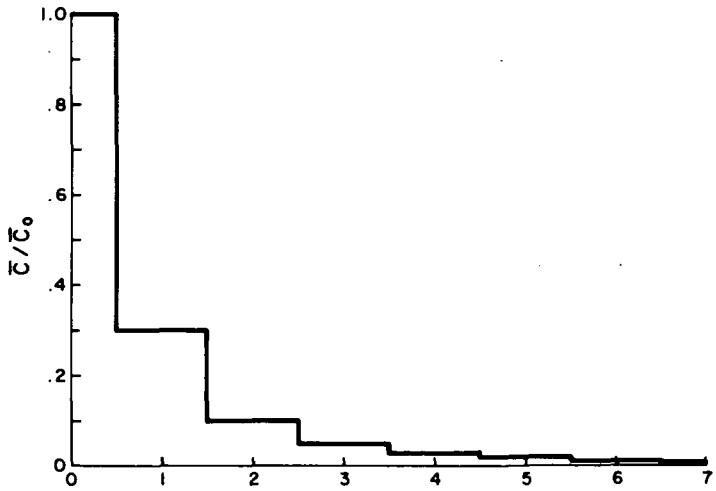

Figure 33. Schematic representation of centerline concentration histories in a turbulence field characterized by short-lived turbulence bursts every T hours and laminar flow between bursts.

Uncertainties in Stratospheric Diffusion Calculations

As must be evident from this entire discussion, the uncertainties of any estimates of turbulent diffusion processes in the lower stratosphere are unacceptably large. Quite literally, these uncertainties extend to the very mechanisms of turbulence generation and decay, a fundamental starting point for any simulation of the time history of the diffusion of SST wake plumes. In addition we have only fragmentary (and somewhat contradictory) information on the parameters to use in any models of these processes, even if we are willing to make some arbitrary choices as to whether diffusion is continuous, periodic, or (as is likely) a result of complicated turbulence histories which encompass the range of intense turbulence bursts induced by unstable gravity and mountain waves to near-laminar flow.

When summarized in a logical way these uncertainties lead to the conclusion that we do not know the "expected" duration of the Phase III wake period to within a factor of ten of its true value. Further, all evidence points to a minimum duration of this phase of several days, and that this duration becomes significant if the Phase III period persists as long as weeks or months. (The analyses which lead to this conclusion are presented in the next section.) Since the latter durations are within the range of uncertainty which must be attached to estimates presently available, it is clear that their significance to CIAP requires harder data on the mechanisms and rates of turbulent diffusion in the lower stratosphere than are now available. Any continuing program designed to refine these estimates for realistic regulation of SST operations in the lower stratosphere should include a measurements program specifically designed to address the questions of mechanisms and rates of dilution of SST plumes.

ESTIMATES OF COUPLED DIFFUSION AND CHEMISTRY OF SOME EXHAUST MATERIALS

With the above analyses of the diffusion of inert exhaust materials in hand, we may now turn attention to the critical problems of chemically active exhaust materials and their reactions with environmental constituents during the Phase III wake period. Since the mere presence of trace amounts of exhaust materials in the stratosphere does not appear to be the cause of any significant environmental alteration (although accumulations of optically significant particulate materials may be important), the major potential environmental impact of SST operations has been identified with the chemical alteration of environmental constituents. In the CIAP analyses of these potential impacts, the problems of ozone

depletion due to the presence of increased (but still trace) amounts of SST-produced water vapor and oxides of nitrogen have emerged as particularly significant subjects for analysis (refs. 1, 3, 7 and 14). In order to provide maximum assistance to CIAP and a focus for the analyses which follow, we have emphasized the NO_x-O_3 reaction system for a study of the coupled effects of diffusion and chemistry during the Phase III wake period.

With this focus, the critical questions which we wish to address are:

1. "Is the chemical efficiency of the NO_x catalytic destruction of O_3 significantly altered during the period when the SST exhaust NO is relatively concentrated in diffusing plumes?" and,

2. "If the answer to 1. is "yes," how long do these effects persist, and what is their significance in the total chemistry during the time the SST exhausts are resident in the stratosphere?"

In posing these questions we are in effect examining the validity and significance of two assumptions made in earlier analyses, one of which states that the chemical efficiency of NO_x destruction of O_3 is always unity, and the other states that, even though this efficiency is less than unity during the Phase III period, this period is short compared with the total residence time in the lower stratosphere, and the effect is therefore negligible in the total problem of O_3 depletion. The following analyses show that the first assumption is highly untenable, and the second assumption cannot be rigorously defended out of present knowledge of the relative durations of the Phase III chemical anomaly and the total residence time of SST exhaust materials. The analyses also show that the combined effects of diffusive mixing and NO_x-O_3 reactions during Phase III can only operate to reduce prior estimates of O_3 depletion, i.e., earlier estimates maximize this effect of SST operations. Offsetting these new insights, however, is the fact that the uncertainties of both these and prior analyses deny a definitive evaluation of the O_3 depletion problem at this time.

The Chemical Model

The following analyses of the combined diffusion and chemistry of NO and O_3 during the Phase III period have utilized calculations made with A.R.A.P.'s coupled, two-dimensional diffusion/chemistry model. This model, which is described in detail in ref. 6, was completed during the early phase of the present study and was developed under partial support from Contract NAS1-11873. In brief, the model solves the nine simultaneous partial differential equations necessary for the solution of the general rate equations for the local concentrations of two reactants, α and β, given on Pages 11-12 of this report. The inputs to the model are 1) the

turbulence field (derived from the turbulence sub-model), 2) the initial concentration distributions for the α and β species, and 3) the reaction rate constants.

Although the model, as presently constructed, is limited to an irreversible binary reaction (and we assume an isothermal reaction as well), the reaction set (the basic NO_x catalytic cycle)

$$NO + O_3 \rightarrow NO_2 + O_2 \tag{56}$$

$$NO_2 + O \rightarrow NO + O_2 \tag{57}$$

can be approximated for model solution by assuming that $NO + NO_2 = NO_x$ is conserved and the ratio of NO to NO_2 is a constant in time. This implies the further assumption that the restoration of NO by reaction (57) is not limited by the supply of O, a questionable assumption in the dark sky, since O is produced primarily by photolysis of O_3 and NO_2. However, under these assumptions the second-order chemical kinetics equations for reactions (56) and (57) may be written

$$\frac{\partial \overline{C}_\alpha}{\partial t} = - k_1(\overline{C}_\alpha \overline{C}_\beta + \overline{C'_\alpha C'_\beta}) \tag{58}$$

and

$$\frac{\partial \overline{C}_\beta}{\partial t} = 0 \tag{59}$$

where we have set $\alpha = O_3$ and $\beta = NO$. Equation (59) assumes that the depletion rate of NO associated with the reaction given in Equation (56) is balanced by the rate of production of NO associated with Equation (57), and follows directly from the assumptions that the sum of $NO + NO_2$ is conserved and the ratio NO/NO_2 is constant in time. Since this is the equivalent of treating NO as a conservative tracer, the resultant calculations of SST NO concentration distributions serve as a surrogate for any conservative exhaust constituent and permit exact comparisons with the results of the nonreactive diffusion calculations described previously.

In the use of this model we have taken $k_1 = 5.5 \times 10^5$ $(ppp\text{-}sec)^{-1}$, a value which may be compared with the value of 1.3×10^5 $(ppp\text{-}sec)^{-1}$ recommended by the CIAP chemistry panel (ref. 15, 16).

Chemical Efficiencies for the NO_x Catalytic Destruction of O_3

In addressing the primary question of the efficiency of the chemical destruction of O_3 by NO via the NO_x catalytic cycle, we note first that two processes are involved when the NO is confined to an intact plume segment in relatively high concentrations. First, the NO reacts with and destroys locally produced O_3 and, second, the environmental O_3 (external to the plume segment) may be diffusively mixed with the NO and is thereby destroyed. In the first process we recognize that the production of O_3 may be anomalously high in the plume segment due, for example, to excessive production of O. However, since NO concentrations are also high, this excess O_3 is destroyed and the result is essentially a "do-nothing" cycle so far as the excess production and destruction of O_3 is concerned. We may, therefore, concentrate on the destruction of only that component of O_3 production which occurs in the normal (nonplume) atmosphere for this phase of the chemical efficiency analysis. For this purpose we assume there is a limiting value of the concentration of NO just capable of destroying O_3 at its local production rate and any excess of NO above this value is inactive in this process.

The second process, on the other hand, depends upon calculations of the rates at which external O_3 and NO are mixed compared with the rate at which they react. To determine the efficiency with which the NO destroys the environmental O_3 we note that the rate of destruction of O_3 in a vertical column of unit cross-section and extending through the plume segment is given by

$$\left[\int_{-\infty}^{\infty} \frac{\partial \overline{C}_\alpha}{\partial t}\, dz\right]_{Col} = -k_1 \int_{-\infty}^{\infty} (\overline{C}_\alpha \overline{C}_\beta + \overline{C'_\alpha C'_\beta})\, dz \qquad (60)$$

Now, the maximum value which $\overline{C}_\alpha$ can attain through the plume is the environmental concentration of O_3 and under this circumstance C'_α must be zero in this column (the O_3 is uniformly mixed). Then the maximum possible rate of destruction of O_3 is

$$\left[\int_{-\infty}^{\infty} \frac{\partial \overline{C}_\alpha}{\partial t}\, dz\right]_{max} = -k_1 \overline{C}_{\alpha e} \int_{-\infty}^{\infty} \overline{C}_\beta\, dz \qquad (61)$$

where $\overline{C}_{\alpha e}$ is the environmental concentration of O_3 and, of course, $\int_{-\infty}^{\infty} \overline{C}_\beta\, dz$ is a measure of the total amount of NO in the vertical column through the plume segment. Since this is the maximum rate at which NO in the plume segment can destroy existing O_3, we may define the chemical efficiency of any combination of NO and O_3 in

the plume by

$$E = \frac{\int_{-\infty}^{\infty} (\overline{C}_\alpha \overline{C}_\beta + \overline{C'_\alpha C'_\beta})\, dz}{\overline{C}_{\alpha e} \int_{-\infty}^{\infty} \overline{C}_\beta\, dz} \tag{62}$$

Chemical Efficiency of NO Destruction of Locally Produced O_3

As a method of estimating the efficiency of plume-bound NO for the destruction of O_3 produced within the plume, we assume the distribution of NO concentration is appropriately specified, at any particular time, by a bivariate normal distribution of the form

$$\overline{C}_\beta = \overline{C}_{\beta o} \exp\left\{ -\tfrac{1}{2}\left(\frac{y^2}{\sigma_y^2} + \frac{z^2}{\sigma_z^2} \right) \right\} \tag{63}$$

where $\overline{C}_{\beta o}$ is the axial concentration on $y = z = 0$ and σ_y^2 and σ_z^2 are the variances of the $\overline{C}_\beta$ distribution in the y and z dimensions, respectively. Further, we assume O_3 is produced at the same rate in all portions of the plume, at a rate appropriate to the nonplume atmosphere (see discussion in previous section), and that there is a concentration of NO, $\overline{C}_{\beta c}$, just capable of destroying O_3 at this rate. Then the efficiency of the NO for the destruction of locally produced O_3, E^*, is the fraction of the total NO which occurs at concentrations less than or equal to $\overline{C}_{\beta c}$ in the plume. Then E^* is given by

$$E^* = 1 - \frac{\int_{-y_c}^{y_c} \int_{-z_c}^{z_c} (\overline{C}_\beta - \overline{C}_{\beta c})\, dy\, dz}{\int_{-\infty}^{\infty} \int_{-\infty}^{\infty} \overline{C}_\beta\, dy\, dz} \tag{64}$$

where (y_c, z_c) are the coordinates of the $\overline{C}_{\beta c}$ concentration isopleth, which go to zero when $\overline{C}_\beta$ is everywhere less than or equal to $\overline{C}_{\beta c}$.

Equation (64) can be solved, using Equation (63), by a conformal mapping of $\overline{C}_\beta$ into the (y, ζ) plane by

$$\zeta^2 = a^2 z^2 \tag{65}$$

where a^2 is defined by $\sigma_y^2 = a^2 \sigma_z^2$. Then

$$\overline{C}_\beta(y, \zeta) = \overline{C}_{\beta 0} \exp\left\{ - \frac{1}{2a^2\sigma_z^2} (y^2 + \zeta^2) \right\} \tag{66}$$

which is a circular distribution of $\overline{C}_\beta$ about the origin of the transformed plume.

$$\overline{C}_\beta(r) = \overline{C}_{\beta 0} \exp\left\{ - \frac{r^2}{2a^2\sigma_z^2} \right\}; \; r^2 = y^2 + \zeta^2 \tag{67}$$

and we note particularly that $\overline{C}_\beta(\infty) = 0$ and

$$\frac{\overline{C}_\beta(r_c)}{\overline{C}_{\beta 0}} = \exp\left\{ - \frac{r_c^2}{2a^2\sigma_z^2} \right\} \tag{68}$$

But

$$\int_{-y_c}^{y} \int_{-z_c}^{z_c} \overline{C}_\beta \, dy \, dz = \pi \int_o^r \overline{C}_{\beta 0} \exp\left\{ - \frac{r^2}{2a^2\sigma_z^2} \right\} dr^2 \tag{69}$$

and for $r = \infty$

$$\int_{-\infty}^{\infty} \int_{-\infty}^{\infty} \overline{C}_\beta \, dy \, dz = 2\pi \, a^2 \, \sigma_z^2 \, \overline{C}_{\beta 0} \tag{70}$$

For $r = r_c$,

$$\int_{-y_c}^{y_c}\int_{-z_c}^{z_c} (\bar{C}_\beta - \bar{C}_{\beta c})\, dy\, dz = \pi \int_o^{r_c} \bar{C}_{\beta 0} \exp\left\{ - \frac{r^2}{2a^2\sigma_z^2} \right\} dr^2$$

$$- 2\pi \int_o^{r_c} \bar{C}_{\beta c}\, r dr \qquad (71)$$

$$= 2\pi\, a^2\, \sigma_z^2\, \bar{C}_{\beta 0}$$

$$\left[1 - \exp\left\{ - \frac{r_c^2}{2a^2\sigma_z^2} \right\} \right] - \pi\, r_c^2\, \bar{C}_{\beta c} \qquad (72)$$

$$= 2\pi\, a^2\, \sigma_z^2\, \bar{C}_{\beta 0} \left[1 - \frac{\bar{C}_{\beta c}}{\bar{C}_{\beta 0}} \right]$$

$$- \pi\, r_c^2\, \bar{C}_{\beta c} \qquad (73)$$

and Equation (64) becomes

$$E^* = 1 - \frac{2\pi\, a^2\, \sigma_z^2\, \bar{C}_{\beta 0} \left[1 - \frac{\bar{C}_{\beta c}}{\bar{C}_{\beta 0}} \right] - \pi\, r_c^2\, \bar{C}_{\beta c}}{2\pi\, a^2\, \sigma_z^2\, \bar{C}_{\beta 0}} \qquad (74)$$

and

$$E^* = \frac{\bar{C}_{\beta c}}{\bar{C}_{\beta 0}} \left[1 + \frac{r_c^2}{2a^2\sigma_z^2} \right] \qquad (75)$$

But

$$\frac{r_c^2}{2a^2\sigma_z^2} = - \ell n \frac{\overline{C}_{\beta c}}{\overline{C}_{\beta 0}}$$

and

$$E^* = \frac{\overline{C}_{\beta c}}{\overline{C}_{\beta 0}} \left[1 - \ell n \frac{\overline{C}_{\beta c}}{\overline{C}_{\beta 0}} \right] \qquad (76)$$

A plot of Equation (76) is given in Fig. 34 and, as can be seen there, the efficiency of plume-bound NO destruction of O_3 is less than 25 per cent until the ratio $\overline{C}_{\beta c}/\overline{C}_{\beta 0}$ goes above 10^{-1}. Since the initial value of this ratio is expected to be around 10^{-4} to 10^{-3}, the efficiency for this process is essentially negligible until the plume has been diluted by a factor of about 10^2 to 10^3. The utilization of plume-bound NO for the destruction of locally produced O_3 is therefore a small fraction of the total NO present in the plume during the first several hundred hours of the plume's existence.

More importantly, perhaps, this calculation provides the first suggestion of an "O_3 hole" in the plume, since within the plume cross-section for which $\overline{C}_\beta > \overline{C}_{\beta c}$ the NO concentration is capable of destroying all of the locally produced O_3. Unless external O_3 is transported into this section of the plume at a rate greater than the rate at which the local excess of NO can destroy it, this portion of the plume should be essentially O_3-free. We now turn attention to this facet of the problem, i.e., the comparative diffusive transport and chemical reaction between the plume-bound NO and the external O_3.

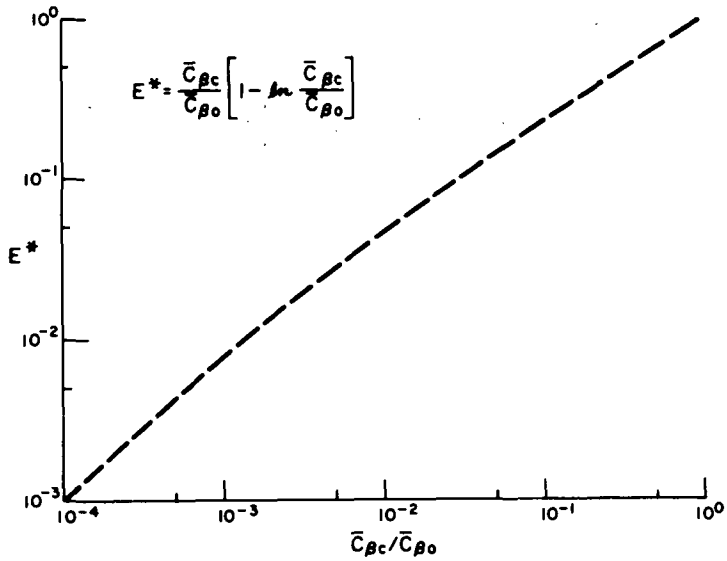

Figure 34. The efficiency of plume-bound NO for the destruction of locally produced O_3 as a function of $\overline{C}_{\beta c}/\overline{C}_{\beta 0}$ where $\overline{C}_{\beta c}$ is the NO concentration which is just capable of destroying O_3 in the nonplume atmosphere and $\overline{C}_{\beta 0}$ is the centerline concentration of NO.

Coupled Chemistry and Diffusion Calculations for Reaction Rates Between SST NO and Environmental O_3

Since the A.R.A.P. coupled diffusion and chemistry model in its present form can handle only two-dimensional (z, t) diffusion calculations, we introduce the assumption that the lateral extent of the plume cross-section is large with respect to the vertical extent and that lateral gradients of concentration are negligible compared with the vertical. The diffusion calculations presented earlier suggest this is an acceptable assumption after the first few hours of plume life.

With this assumption, we have exercised the invariant diffusion/chemistry model for various choices of the turbulence field and for various plume cross-sections representative of the diffusive life history of the NO plume during the Phase III wake period. These calculations have been summarized in terms of the chemical efficiency of NO destruction of environmental O_3 and the controlling physical causes when this efficiency is less than one.

To illustrate these calculations and the basic mechanisms at work, the results of one calculation are given in detail in Figs. 35 and 36. The conditions chosen for this calculation are 1) a stably stratified atmosphere, and 2) vertical turbulent rms velocity component of 0.143 m/sec ($\overline{w'^2} = 0.02\ m^2/sec^2$); the NO plume had a centerline concentration of 1.8×10^{-7} kg/m^3 and a vertical thickness of slightly more than 200 meters. The environmental concentration of O_3 (external to the plume) was taken as 2×10^{-7} kg/m^3 (~ 2 ppm). The "equilibrium" profiles of NO and O_3 concentrations for these conditions are shown on the left-hand side of Fig. 35. (Only the upper half of the full plume is plotted; since the plume is symmetrical about its axis, there is, of course, a mirror image of all of these quantities along the negative z axis.) On the right-hand side of this figure we have plotted the calculated chemical reaction rate (O_3 depletion rate) as a function of height, first including the "mixedness" term, $\overline{C'_\alpha C'_\beta}$, and then, for comparison, the reaction rates calculated for the mean values of the concentration of NO and O_3.

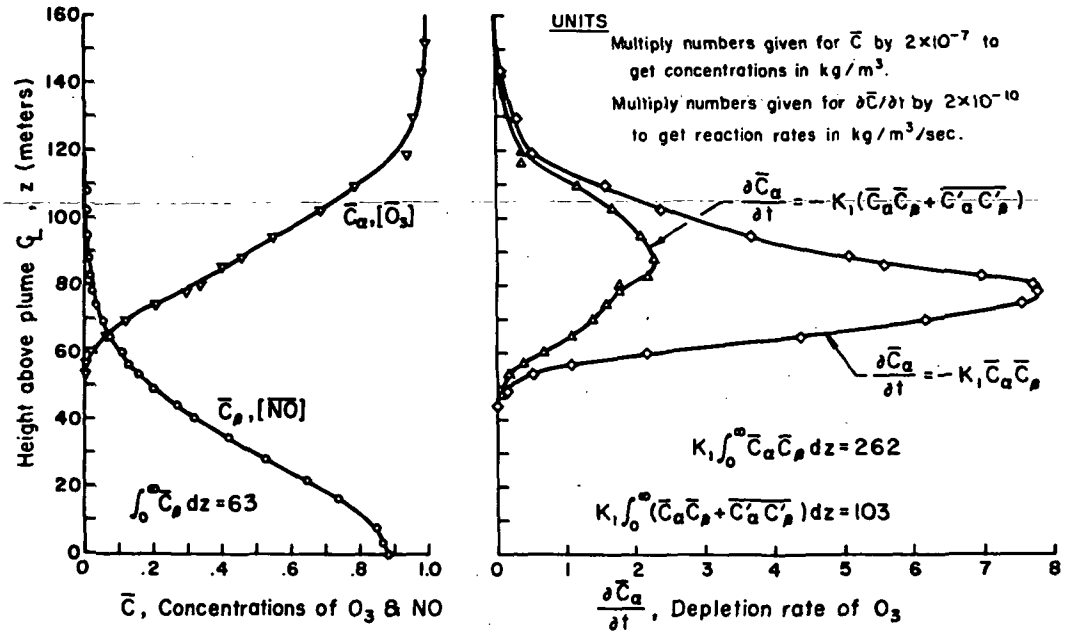

Figure 35. Calculated vertical profiles of NO and O_3 concentration in the half-plume and the chemical reaction rate for the depletion of O_3 for t = 150 sec. The reaction rate based on mean values of concentration only is shown to illustrate the effect of mixedness on the reaction rate.

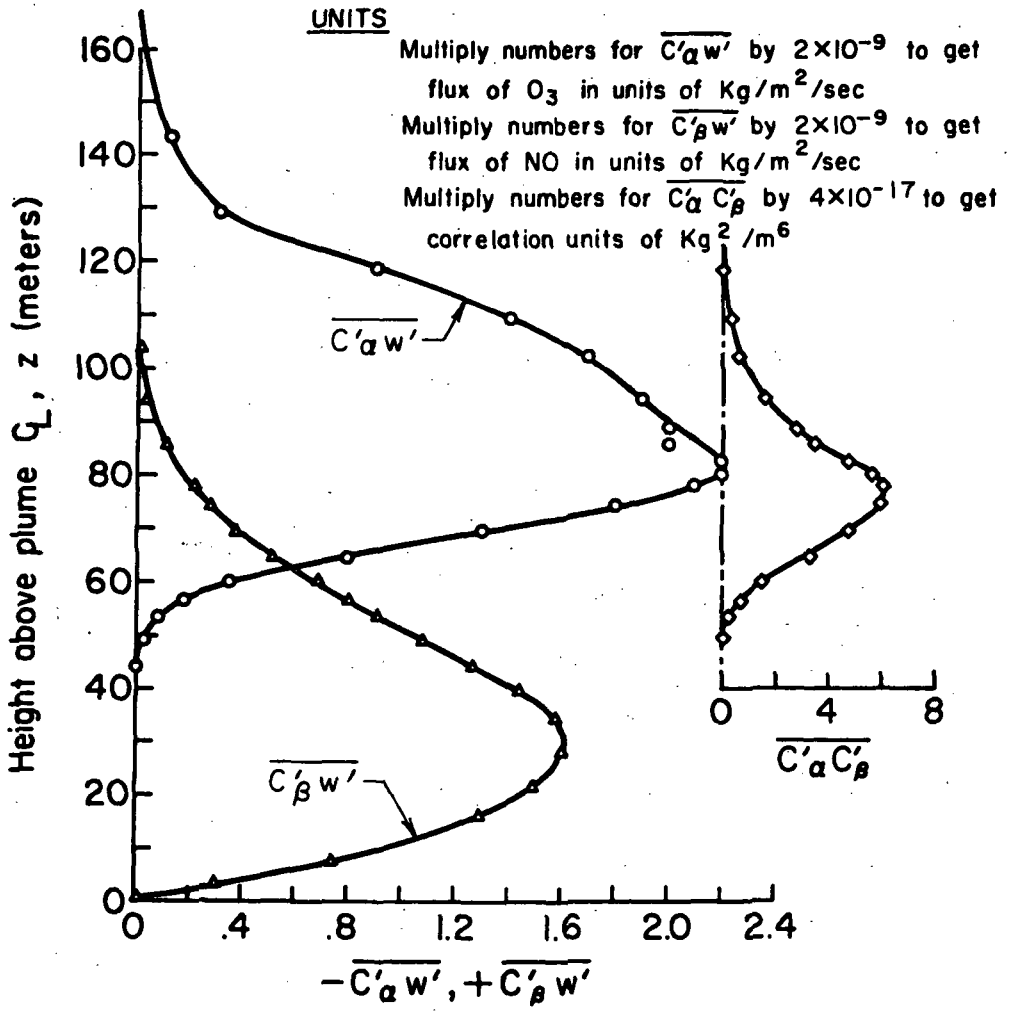

Figure 36. Calculated vertical profiles of the vertical turbulent fluxes of NO (β) and O_3 (α) and the mixedness correlation of their concentration fluctuations for the case shown in Fig. 35.

From these results we can quickly discern that from the plume axis up to 50 m the plume is O_3-free; the combination of diffusive mixing and chemical reaction has created an "O_3-hole" in the core of the plume. Second, the chemical reaction rate profiles show the destruction of O_3 occurs only in the outer edges of the NO plume and, due to a lack of intimate local mixing of the NO and O_3, the total reaction rate is only about one third the rate predicted by mean value chemical kinetics. From these results we can also deduce that the efficiency of the NO destruction of O_3 is (recall Equation (62), $E \simeq 2 \times 10^{-3}$, i.e., only 2/10ths of one per cent of the plume NO is involved in the destruction of environmental O_3!

The associated vertical profiles of the turbulent flux of NO and O_3 are shown on the left-hand side of Fig. 36, and the "mixedness" factor profile is shown on the right-hand side of this figure. The profile of $\overline{C'_\alpha w'}$ shows clearly that the turbulent flux of O_3 into the plume is completely offset by chemical depletion below about 50 meters. Similarly, the mixedness limitation on the chemical reaction rate is a maximum at the height at which turbulent diffusion is most strongly "folding" the O_3 into the NO at the edge of the NO plume.

We can now examine the relative effects of the diffusion limitation and the mixedness limitation on the chemical efficiency of this system as follows: Let

$$R^* = k_1 \overline{C}_{\alpha e} \int_o^\infty \overline{C}_\beta \, dz$$ (the maximum possible reaction rate in the half-plume)

$$R = k_1 \int_o^\infty (\overline{C}_\alpha \overline{C}_\beta + \overline{C'_\alpha C'_\beta}) \, dz$$ (the calculated reaction rate in the half-plume)

$$M = -k_1 \int_o^\infty \overline{C'_\alpha C'_\beta} \, dz$$ (the mixedness component of the calculated reaction rate in the half-plume)

$$D = R^* - (R + M)$$ (the diffusion component of the difference between the maximum and the calculated reaction rate in the half-plume)

Then, by definition,

$$E = \frac{R}{R^*} = 1 - L_D - L_M \qquad (77)$$

where $L_D = D/R^*$ and $L_M = M/R^*$. For the example given above

$$R^* = 126 \times 10^{-7} \text{ kg/sec}$$

$$R = 206 \times 10^{-10} \text{ kg/sec}$$

$$M = 318 \times 10^{-10} \text{ kg/sec}$$

$$D = 125.5 \times 10^{-7} \text{ kg/sec}$$

$$E = 1.63 \times 10^{-3}$$

$$L_M = 2.6 \times 10^{-3}$$

$$L_D = .996$$

The diffusion limitation accounts for essentially all of the chemical efficiency deficit calculated for this case. In fact, the case just discussed is appropriate to present estimates of SST exhaust emissions of NO about one hour after fly-by, and they point very clearly to a chemical reaction system completely dominated by diffusive mixing. The net result is a marked reduction of the NO destruction of O_3 compared with the rate calculated under the assumptions of uniform mixing of O_3 through the plume and mean value chemical kinetics. In a very real sense these results indicate that the NO plume is self-shielding so far as environmental O_3 destruction is concerned; it is as though the NO were placed in the stratosphere in a slightly permeable shell which expands and erodes with time. To study the importance of this to CIAP, we now turn to estimates of the rate at which this expansion and erosion occurs and its control of the efficiency of NO destruction of O_3.

The Dependence of Chemical Efficiency on Turbulence Intensities and NO Plume Concentrations During Phase III

In order to estimate the chemical efficiency of NO destruction of O_3 during the Phase III wake period and for a range of turbulence conditions, the A.R.A.P. coupled diffusion/chemistry model was run for nine combinations of turbulence intensity, q^2, and plume widths, σ_y. The range of q^2 was from 10^{-2} m^2/sec^2 to 10 m^2/sec^2, and the range of σ_y was from 10^2m to 10^4m. The vertical thickness of the plume was held at $\simeq$ 200 m (σ_z = 50 m), and the centerline concentration of NO was taken as 10^{-7} kg/m^3 when $\sigma_y = 10^2$ m. (Additional calculations have shown that there is a weak dependence of E on σ_z which is to be studied further, but, which is apparently of negligible importance in the present analyses.)

Since the concentration of NO in the plume is essentially inversely proportional to σ_y, this variable may be treated as a measure of the concentration of NO, controlled by either the lateral diffusion of the SST plume or by the variation of the NO emission rate. While we shall emphasize a constant emission rate and interpret these results in terms of diffusion of the NO plume during Phase III, they are equally appropriate to estimates of the effects of increasing or reducing the NO emission rate from SST's. In the latter case, one simply assumes the dimensions of the plume are constant and the emission rate varies inversely as σ_y.

The results of these calculations of E, L_M, and L_D are shown in Figs. 37, 38 and 39 respectively, and the dependence of chemical efficiency and the mechanisms which cause this efficiency to depart from one during Phase III are immediately evident. As was to be expected, E varies from less than 0.05 when $q^2 = 10^{-2}$ m^2/sec^2 and $\sigma_y = 10^2$m to very nearly 1.0 when $q^2 = 1$ m^2/sec^2 and $\sigma_y = 10^4$m. For the most part E depends more strongly on the concentration (or plume width) than it does on the intensity of turbulence. The exception to this statement is found when the concentrations of NO are relatively high (σ_y is small). In this case E depends about equally on the concentration of NO and the intensity of turbulence.

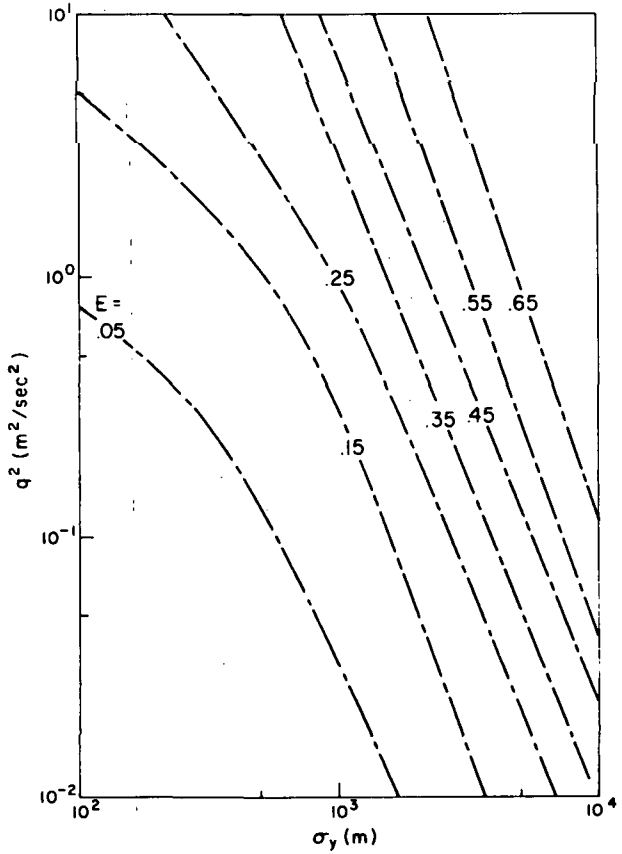

Figure 37. Calculated efficiencies of NO destruction of environmental O_3 as a function of turbulence intensity q^2 and the lateral dimensions of the NO plume, σ_y .

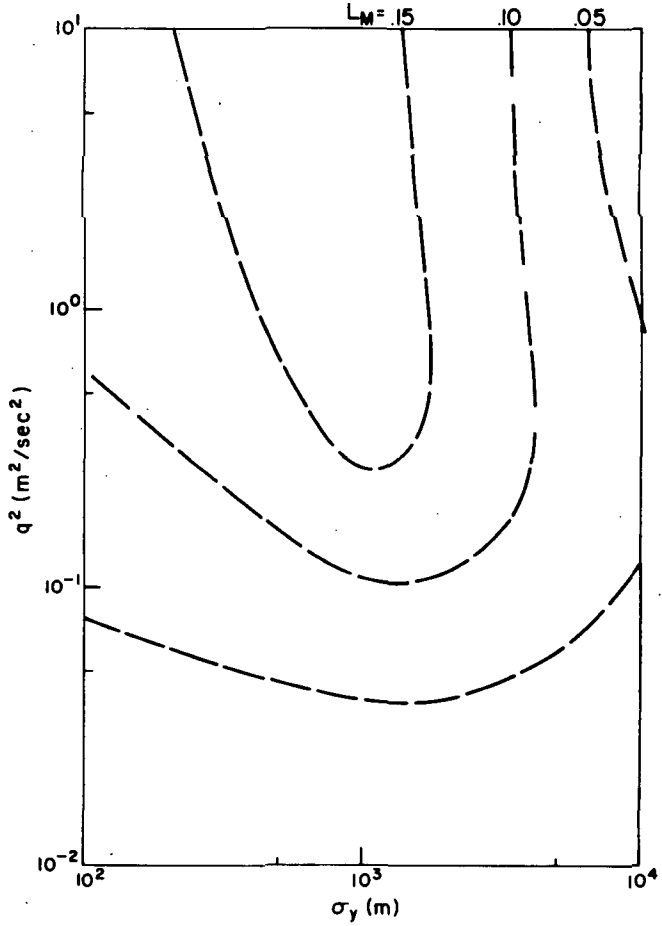

Figure 38. The contribution of the mixedness limitation to the efficiency deficit for NO destruction of O_3 as a function of turbulence intensity, q^2 , and plume width, σ_y .

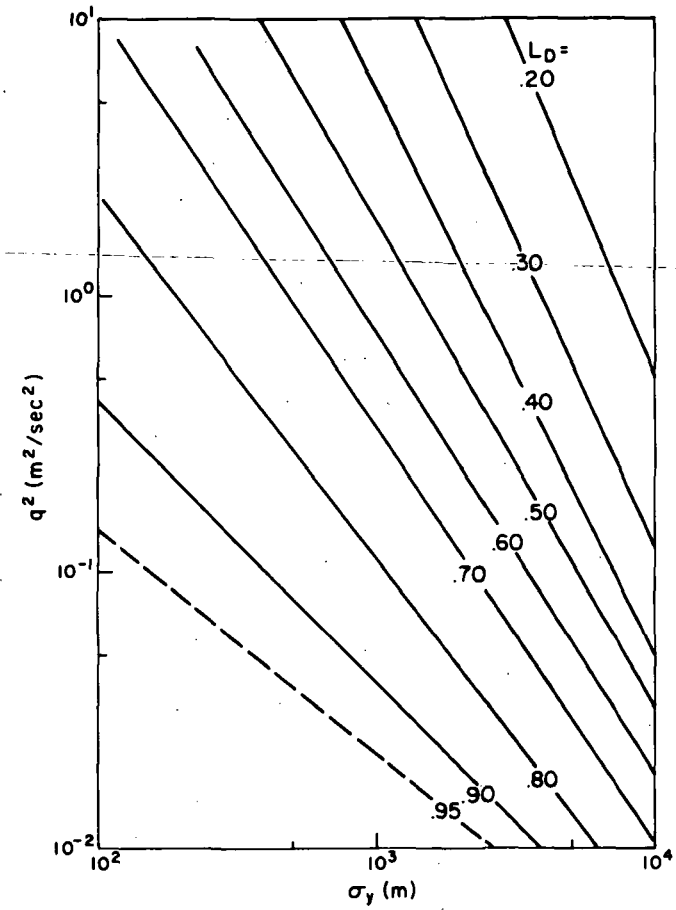

Figure 39. The contribution of the diffusion limitation to the efficiency deficit for NO destruction of environmental O_3 as a function of turbulence intensity, q^2 , and plume width, σ_y .

The relative contributions of the mixedness limitation, L_M, and the diffusion limitation, L_D, to E are clearly shown in Figs. 38 and 39. In all cases the diffusion limitation dominates these two effects. In its region of maximum value ($\sigma_y \sim 10^3$m and $q^2 > 1$ m^2/sec^2) L_M never contributes more than one third to the efficiency deficit. However, note that the mixedness limitation acts to counter the diffusion limitation; if L_M is neglected, E will be overestimated.

With these calculations in hand we may now make some preliminary estimates of the overall effect of diffusion and mixedness limitations on the NO-O_3 reaction during Phase III. To do so, we assume that the initial axial concentration of NO in the plume is 2 ppm (the immediate post-vortex region of the plume) and that the NO concentration is diluted by diffusive mixing until it reaches a background concentration of 2×10^{-4} ppm. At this time we presume the NO is in chemical equilibrium with the locally produced O_3 and diffusive transport of the O_3 is no longer influenced by the presence of excess NO above background.

Now, consider the two diffusion histories designated as Case 3 and Case 4 and shown in Figs. 23 and 24. For the first (Fig. 23) the NO concentration reaches background levels at about 2×10^6 sec in a turbulence field of $q^2 = 2.5 \times 10^{-2}$ m^2/sec^2. In the second case (Fig. 24) the the NO concentration reaches background levels at $t \simeq 4 \times 10^6$ sec in a turbulence field of $q^2 = 8.5 \times 10^{-3}$ m^2/sec^2. Using the predicted values of σ_y as a function of time for these cases, we may enter Fig. 37 and read off estimates of E as a function of time. The resulting time histories of E for these two cases are shown in Fig. 40.

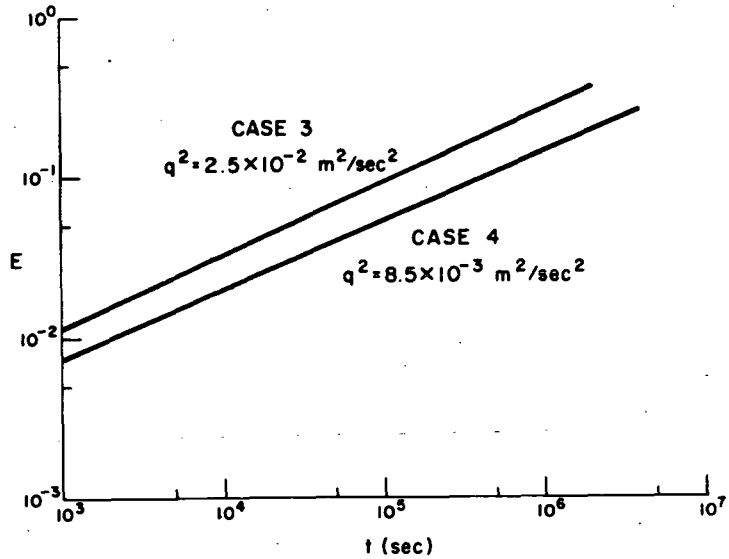

Figure 40. Estimated time histories of the chemical efficiency of NO destruction of O_3 during the time required to dilute the NO plume by a factor of 10^4.

From these examples we may estimate that the duration of Phase III is 600 to 1200 hours, and the chemical efficiency of NO destruction of environmental O_3 during this time is between 10 and 20 per cent. Recall that we have assumed light but continuous turbulence fields for these calculations - any individual plume segment which encounters a strong turbulence burst during Phase III period will, of course, follow a different diffusion and chemical efficiency history. On the other hand, plume segments may frequently find themselves in essentially laminar flow and these will, of course, diffuse more slowly (if at all) and exhibit much lower chemical efficiencies during these periods. At best, the examples cited above may be considered a weighted mean among these diverse Phase III histories, and therefore provide "expected" values of Phase III durations and chemical efficiencies. Improvement upon these estimates depends upon much more knowledge of the turbulence regimes in the lower stratosphere than we now possess.

Implications for Overall NO Destruction of O_3

The above estimates of NO destruction of O_3 during Phase III take on their real significance for CIAP evaluations only when they are appropriately incorporated in estimates of the effects produced by SST exhausts during their entire residence time in the lower stratosphere. Since we have not made any definitive assessment of this residence time, we can only note the range of estimates made by others, which extend from something less than 6 months to something greater than a year. If we assume the SST NO is fully active in the destruction of O_3 following Phase III, we may estimate the overall effect of Phase III from the relationship

$$\bar{E}(T_R) = 1 - \frac{T}{T_R}\,(1 - E(T)) \qquad (78)$$

where $\bar{E}(T_R)$ is the chemical efficiency for the entire residence time, T_R, T is the duration of Phase III, and $E(T)$ is the chemical efficiency during Phase III. From the above estimates, T is of the order of 10^3 hours and $E(T)$ is about 0.15. Then

$$\bar{E}(T_R) = 1 - \frac{10^3}{T_R}\,(0.85) \qquad (79)$$

If T_R is as little as 2×10^3 hours (~ 3 months), $\bar{E}(T_R) \simeq 0.60$. If T_R is of the order of one year (~ 10^4 hours), $\bar{E}(T_R) \simeq 0.92$. In the latter case, the overall effect of Phase III chemistry limitations is quite negligible; in the first case the effect is the equivalent of nearly halving the proposed SST fleet!

Experimental Verification and Refinements of These Results

The foregoing analyses of the structure of turbulence, turbulent diffusion processes, and the combined mechanisms of diffusion and chemistry, as these relate to the environmental impact of SST operations in the lower stratosphere, can be accepted as conclusive only when appropriately validated against direct observations. As has been noted throughout this report, present observational data are adequate to this important task only if uncertainties of orders of magnitude in critical processes and of factors of 2 to 10 in estimates of environmental effects (e.g., the depletion of O_3) are acceptable and useful. The paucity of appropriate data is hardly surprising, since observations which have been made have been quite different applications. For example, measurements of turbulence intensities and structure have, until very recently, been designed to provide criteria for structural requirements on aircraft expected to fly in this region of the atmosphere. It is quite appropriate to use aircraft as measurement platforms for this purpose and to emphasize the measurement of the relatively severe levels of turbulence which would be significant in structural failures. These data are only marginally useful in determining the diffusion of exhaust materials, however, since the threshold values of turbulence measured are too large and the method of measurement (fly-bys) precludes any definitive specification of the turbulence history to which these exhaust materials are subjected.

Similarly, the estimates of chemical reactions and their consequences for environmental states are handicapped by the lack of adequate measurements of the natural magnitude and time- and space-variabilities of the concentrations of key chemical species. Any attempt to measure directly the chemical consequences of injected exhaust products must contend with these background and "noise" levels.

If the reduction in uncertainties of the estimates of environmental impacts of SST operations is important to the regulation of their operations, then the hard data appropriate to these analyses must be obtained. In this regard, and aside from their value in providing first estimates for CIAP evaluations, the models described here are extremely valuable in the design of experimental measurements which will clarify key processes and serve to validate predictions of the environmental consequences of SST operations. These are, of course, tasks beyond the present objectives of CIAP, but it seems equally clear that one of CIAP's responsibilities is to prescribe what more needs to be done. Given the intensive scoping of the problems, analyses, and preliminary estimates which CIAP has accomplished, the stage is set for a thoughtful and balanced prescription of requirements for refinement of these estimates.

CONCLUSIONS

In conclusion, we may summarize the results of this study to date by answering the questions posed in the introductory remarks. The first question was, "During the Phase III wake period, is the chemical behavior of the SST exhaust materials significantly different from their behavior after they are well-mixed in the stratospheric environment?" The answer is an unequivocal "yes," if the chemical reaction rates are fast with regard to the diffusion rates encountered in the lower stratosphere.

The second question was, "If the answer (to the first question) is "yes," what is the nature and magnitude of this effect(s), and how long does it last?" The answers to this question are several, and they may be summarized as follows:

1. During Phase III the reaction of NO with O_3, via the NO_x catalytic cycle, for the destruction of O_3 is strongly inhibited by the limitations of diffusive mixing between the NO plume and the environmental O_3, and by the relatively small local production of O_3. As a result of these limitations, the efficiency of NO destruction of O_3 during Phase III is probably around 15 per cent, and may be less.

2. Best estimates of exhaust emissions of NO and of the diffusive properties of the stratosphere suggest Phase III should, on the average, persist for about 1000 hours, but this estimate is uncertain within a factor of five to ten of that number.

The third question posed was, "Do the combinations of the nature, magnitude, and duration of the chemical behavior of SST exhausts during Phase III significantly alter estimates of the impact of SST fleet operations on the stratospheric environment?" A logical assembly of the analyses directed to the first two questions (again in the context of NO destruction of O_3), and assuming the post-Phase III chemical behavior is properly portrayed by classical chemical kinetics, the answer to this question is that there may be a significant effect, but estimates of this effect are uncertain within a factor of two to five. From what we know now with regard to the multiple factors which enter into these estimates, the Phase III chemistry anomaly may reduce the previous O_3 depletion estimates by either as much as 80 to 90 per cent or by as little as 10 per cent. There is presently little basis for choice within this range.

It is only fair to note that the significance of these results depends strongly upon the validity of prior analyses of the overall impact of NO on O_3 and on estimates of expected exhaust emissions.

If, in fact, further analyses of the multiple chemical processes which govern the balance of O_3 in the stratosphere significantly reduce estimates of the depletion of O_3 during the entire residence time of SST exhausts, then Phase III effects tend to become unimportant. On the other hand, increases in these large-scale effects enhance the Phase III anomaly. Similarly, reductions in SST exhaust emissions operate to minimize the Phase III anomaly and reduce its importance in the CIAP evaluation. For example, a reduction of NO emissions to 10 per cent of present estimates and an accompanying increase of the SST fleet by a factor of ten shifts the overall problem to the large-scale effects since the anomalous behavior during Phase III is reduced while the total emissions are kept constant. This latter consideration says, in effect, that environmental effects are not on a one-to-one relationship with total SST emissions, and caution should be used in evaluating any extrapolations of these effects based on such an assumption.

Finally, an attempt has been made in this report to present results of the use of invariant model analyses in sufficient detail to be useful to other modelers. In particular, the presentations of the simulations of turbulence structure and the diffusive properties of stratospheric flows are sufficiently detailed to permit direct use of these tools by the reader. As a minimum, these analyses permit a consistency check on the properties of turbulence and the mean wind and temperature fields used in any diffusion calculations. Unhappily, the models do not prescribe the forcing functions which dictate the history of turbulence and all its consequences, but they do provide best estimates of the results, given our best guesses as to what these functions are. One of our chores is to convert these "guesses" into facts.

REFERENCES

1. Man's Impact on the Global Environment: Assessment and Recommendations for Action. Report of the Study of Critical Environmental Problems (SCEP), MIT Press, 1970.

2. Inadvertent Climate Modification. Report of the Study of Man's Impact on Climate (SMIC), MIT Press, 1971.

3. Johnston, Harold: Reduction of Stratospheric Ozone by Nitrogen Oxide Catalysts from Supersonic Transport Exhaust. Science, vol. 173, August 6, 1971, pp. 517-522.

4. Donaldson, Coleman duP. and Hilst, Glenn R.: Effect of Inhomogeneous Mixing on Atmospheric Photochemical Reactions. Environmental Science and Technology, vol. 6, Sept. 1972, pp. 812-816.

5. Donaldson, Coleman duP.: Atmospheric Turbulence and the Dispersal of Atmospheric Pollutants. EPA-R4-73-016a, March 1973.

6. Hilst, Glenn R., et al.: The Development and Preliminary Application of an Invariant Coupled Diffusion and Chemistry Model. A.R.A.P. Report No. 193, (also NASA CR- 2295), May 1973.

7. Hilst, Glenn R.: Solutions of the Chemical Kinetic Equations for Initially Inhomogeneous Mixtures. Second Conference on the Climatic Impact Assessment Program, Nov. 1972, pp. 351-357.

8. Lewellen, W. S. and Teske, M.: Prediction of the Monin - Obukhov Similarity Functions for an Invariant Model of Turbulence. A.R.A.P. Report No. 185, to be published in the J. of Atmos. Sciences, October 1973.

9. Ashburn, E. V., et al.: High Altitude Gust Criteria for Aircraft Design. Tech. Report AFFDL-TR-70-101, October, 1970.

10. Kellogg, W. W.: Diffusion of Smoke in the Stratosphere. J. Meteorol., vol. 13, June 1956, pp. 241-250.

11. Rosenberg, N. W., Good, R. E. and Zimmerman, S. P.: Transport Measurements in the Stratosphere. Second Conference on the Climatic Impact Assessment Program, Nov. 1972, pp. 247-253.

12. Bauer, Ernest: Dispersion of Tracers in the Atmosphere: Survey of Meteorological Data. Paper P-925, IDA Contract DAH 73 0200 Task T-90, February 1973.

13. Lilly, D. K.: Draft Copy, DOT/CIAP Monograph III, March 1973.

14. Grobecker, A. J.: Chairman's Address: The DOT Climatic Impact Assessment Program. Proceedings of the Survey Conference (CIAP), February 1972.

15. Johnston, H. and Crosley, H.: CIAP Monograph I. J. Chem. Phys. vol. 22, 1954, pp. 689; ibid vol. 19, 1951, pp. 799.

16. Garvin, David, ed.: Chemical Kinetics Data Survey IV. Preliminary Tables of Chemical Data for Modelling of the Stratosphere. CIAP Interim Report NBSIR 73-203, May 1973.